MICROCOPY RESOLUTION TEST CHART
NATIONAL BUREAU OF STANDARDS-1963-A

LEVEL

FINAL REPORT

AFOSR Contract F44620-76-C-0083

"Applications of Rayleigh Scattering to Turbulent Flows

with Heat Transfer and Combustion"

Principal Investigators: L. Talbot
F. Robben

University of California, Berkeley

May 6, 1980

80 7 14 016

REPORT DOCUMENTATION PAGE	READ INSTRUCTIONS BEFORE COMPLETING FORM

1. REPORT NUMBER AFOSR-TR-80-0535	2. GOVT ACCESSION NO. AD-A086 060	3. RECIPIENT'S CATALOG NUMBER

4. TITLE (and Subtitle) APPLICATIONS OF RAYLEIGH SCATTERING TO TURBULENT FLOWS WITH HEAT TRANSFER AND COMBUSTION	5. TYPE OF REPORT & PERIOD COVERED Final Report 1 Mar 78-29 Feb 80
	6. PERFORMING ORG. REPORT NUMBER

7. AUTHOR(s) L./Talbot F./Robben	8. CONTRACT OR GRANT NUMBER(s) F44620-76-C-0083

9. PERFORMING ORGANIZATION NAME AND ADDRESS UNIVERSITY OF CALIFORNIA, BERKELEY DEPARTMENT OF MECHANICAL ENGINEERING BERKELEY, CA 94720	10. PROGRAM ELEMENT. PROJECT, TASK AREA & WORK UNIT NUMBERS 2307A3 61102F

11. CONTROLLING OFFICE NAME AND ADDRESS AIR FORCE OFFICE OF SCIENTIFIC RESEARCH/NA BLDG 410 BOLLING AIR FORCE BASE, D.C. 20332	12. REPORT DATE May 6, 1980
	13. NUMBER OF PAGES 66

14. MONITORING AGENCY NAME & ADDRESS(if different from Controlling Office)	15. SECURITY CLASS. (of this report) UNCLASSIFIED
	15a. DECLASSIFICATION DOWNGRADING SCHEDULE

16. DISTRIBUTION STATEMENT (of this Report)

Approved for public release; distribution unlimited.

17. DISTRIBUTION STATEMENT (of the abstract entered in Block 20, if different from Report)

18. SUPPLEMENTARY NOTES

19. KEY WORDS (Continue on reverse side if necessary and identify by block number)

FLAME PROPAGATION
COMBUSTION IN TURBULENT FLOWS
RAYLEIGH SCATTERING
LASER ANEMOMETRY

20. ABSTRACT (Continue on reverse side if necessary and identify by block number) Rayleigh scattering has been developed as a diagnostic technique and used in conjunction with Laser Doppler Anemometry to study two reacting flows; the interaction of a Kármán vortex street with a flame, and the interaction of grid-produced turbulence with a flame. It was found that one of the dominant effects of heat release and flow dilatation is to decrease turbulent kinetic energy, and to increase the integral scales of the turbulence. Flame holder drag is found to have a major effect on the flow-field behind the flame. The Markstein model for the effect of wrinkling on flame stability appears to be in qualitative agreement

DD FORM 1473 EDITION OF 1 NOV 65 IS OBSOLETE

(cont'd from Page 1)   Abstract

with the results of the vortex interaction experiments.

1. INTRODUCTION

The profound effect of fluid mechanical turbulence on combustion, as evidenced by large increases in effective flame speeds and volumetric burning rates, has been the subject of theoretical and experimental investigations for at least 100 years (see e.g. the review by Andrews et al., 1975). From an experimentalist's viewpoint, progress has been critically impeded by the lack of diagnostic probes which could provide measurements of the statistical nature of velocity, density (temperature) and concentration fields. From the theoretical point of view, advances in the understanding of turbulent flows with combustion have awaited developments in the theory of isothermal turbulent flows. Under this AFOSR contract, we have sought both to develop Rayleigh scattering as an optical diagnostic for density in turbulent flows with combustion, and to investigate flame propagation in turbulent flows. The diagnostic has now been developed with sufficient temporal and spatial resolution to provide statistical data to complement other optical measurement techniques such as Laser-Doppler Anemometry (LDA).

Additional studies in turbulent combustion using Rayleigh scattering are being carried out in our group with support from the Basic Energy Science Division of the Department of Energy. The results reported by Cheng et al. (1979, 1980) and Talbot et al. (1980) indicated that Rayleigh scattering and LDA may be successfully applied to provide information on the interaction of combustion and turbulence in boundary layers. These results shall not be further discussed here. In addition to these studies, Rayleigh scattering has been used to study the effect of catalytic surfaces in a laminar heated boundary layer (Schefer et al., 1980).

The effect of fluid mechanical turbulence on transport phenomena is one of the central problems of fluid mechanics. Turbulence results from the amplification and distortion of hydrodynamic instabilities. Due to the non-linear nature of hydrodynamic interactions, disturbance energy is distributed over a large spectrum of length scales. In high Reynolds number flows turbulent kinetic energy is generated at the largest length scales and dissipated at the smallest, Kolmogorov, scales allowed by viscosity. For large enough Reynolds number these two processes are essentially independent.

Damkohler (1940) was the first to study the effect of turbulence and its associated length scales on flame propagation. He defined two regimes for this combustion problem. The first regime, corresponding to the flame structure commonly called the wrinkled laminar flame, occurs when the turbulence length scales are greater than the laminar flame thickness. In this regime, found at relatively low Reynolds numbers, the increase in effective flame propagation speed is simply attributed to the wrinkling of the flame surface and augmentation of the surface area of the reaction zone. The second regime of turbulent flame propagation occurs for Reynolds numbers in which turbulence length scales are smaller than the reaction zone thickness. Under these conditions, transport within the reaction zone is directly affected by turbulent processes. Spalding (1957), for example, assumed that the effect of turbulence may be modelled by replacing molecular diffusivities with turbulent eddy diffusivities. Numerous phenomenological models have been reported based upon the ideas of Damkohler (1940). An extensive review is given by Andrews et al. (1975). The early models, which have had limited success in correlating available data, are similar

to early turbulence models with their appeal to mixing length and other ad-hoc arguments. More systematic models will be discussed below.

A severe limitation in testing the validity of combustion models has been the lack of accurate data on turbulent burning speeds. Smith and Gouldin (1977) have shown that such measurements may be greatly in error unless the propagation speed is measured locally at the flame front. Despite such problems, comparisons between models and existing data (Andrews et al., 1975) have helped researchers focus on a number of key questions. These include questions concerning 1) the criteria for the existence of a wrinkled laminar flame, 2) effect of length scale distribution on turbulent flame speed, 3) effect of combustion on turbulent kinetic energy, and 4) proper correlation parameters for turbulent flame speeds.

Recent models of turbulent flame propagation have sought to more systematically calculate the effect of turbulence on combustion using the conservation equations (Clavin and Williams, 1979; Bray and Libby, 1976; Libby and Bray, 1977). Clavin and Williams (1979) developed a statistical theory for the structure and propagation velocity in turbulent flows with length scales large compared with the laminar flame thickness. The analysis involves a regular perturbation for small value of the ratios of the laminar flame thickness to the turbulent length scale. This approach is superior to that of previous phenomenological models in that it is not necessary to introduce arbitrary assumptions concerning the flame shape. The turbulent burning rate appears as a solution to an eigenvalue problem for a given fluctuating flow field. The model is limited in that the density change associated with heat release is neglected. However, the qualitative features resulting from the

method of formulation are still of interest. The model predicts that the burning speed will be a function of the laminar flame speed and turbulence intensity; however, no dependence on length scale is indicated. (We note this contradicts the correlation of Andrews et al., 1975). Since the velocity flow field is assumed to be given, no information on the effect of combustion on turbulent kinetic energy may be obtained.

Bray and Libby (1976) in a study of turbulence-combustion interactions in premixed flows calculated the effect of heat release on turbulent flame speed and kinetic energy. The statistical model employs density weighted averaging to take into account variations in density due to heat release. A probability density function dependent on a single reaction progress parameter and location is used to compute statistical moments related to concentration fluctuations. The model predicts that turbulent kinetic energy will be reduced by dilatation effects for flames nearly normal to the upstream flow direction. At higher angles, turbulent kinetic energy is predicted bo be increased due to shear. In addition the thickness of the turbulent flame is predicted to be proportional to the integral scale of the upstream turbulence. The flame speed, as in Clavin and Williams (1979), is found to be independent of the upstream length scale. In a subsequent paper, Libby and Bray (1977) predict that the effects of variations in density are important in the modelling of turbulent transport terms such as the Reynolds stress.

In our studies of turbulent flame propagation, we have used Rayleigh scattering and LDA in the turbulent regime for combustion corresponding to the wrinkled laminar flame. Two flow configurations

have been investigated 1) flame propagation in grid-induced turbulence and 2) the interaction of a Kármán vortex street with a plane flame front.

In the first study, a V-shaped C_2H_4/air flame was stabilized on a rod downstream of a grid used to generate turbulence. This configuration is convenient for the study of turbulent flame propagation since the characteristics of the isothermal flow field have been studied by numerous investigators. Both Rayleigh scattering and LDA measurements have been obtained upstream and through the flame front. A time series analysis of the velocity and density data was performed in which statistical moments, power spectra, and autocorrelation and probability density functions were calculated. For flame fronts at relatively large angles to the flow, the effect of heat release and flow dilatation is to decrease turbulent kinetic energy as suggested by Libby and Bray (1977). At smaller flame angles, however, no increase in turbulent kinetic energy was detected. This is in contradiction to Libby and Bray (1977) and would seem to indicate that their assumption of undeflected streamlines is a poor approximation for unconfined flames. In addition, for oblique flames, the measured increases in turbulent kinetic energy due to the wake of the flame holder suggests that previous results such as that of Smith and Gouldin (1977) are more representative of the interaction of a flame front with wake-generated turbulence. The effect of increased viscosity due to heat release is to increase length scales behind the flame front. Our statistical analysis of density fluctuations indicates that models using a probability density approach are appropriate. Detailed results are discussed in section 3.

The second problem, the interaction of a vortex street with a flame front, represents an idealization of the turbulence-combustion interaction process. In this study, the grid is replaced by a single cylinder which sheds vortices at a fixed frequency. Thus we are able to isolate the effects of the passage of a single, two-dimensional eddy through the reaction zone. This is in contrast to the interaction with grid-induced turbulence in which a three-dimensional spectrum of eddies are present. Using a hot-wire upstream of the flame, we are able to monitor the shedding of eddies. This allows us to use phase-locked averaging techniques with Rayleigh scattering and LDA measurements to provide an instantaneous picture of the velocity flow field. In effect we are able to measure the geometry of the wrinkled laminar flame. The effect of heat release on vortices as they pass through the reaction zone may also been determined.

These results have been compared qualitatively with a potential flow solution in which the flame front is modelled as a line source of specific volume (see Karasalo et al., 1980, Appendix A). Our data indicate that the main characteristics of the kinematics of the flow field are well accounted for by such a model. The data suggest, however, that modifying the solution to include the random vortex method (Chorin, 1973) may provide a more realistic description of the effects of heat release on eddies as they pass through and behind the reaction zone.

Accession For

NTIS &.JA&I	✓
DDC TAB	☐
Unannounced	☐
Justification	

By____

Distribution/

Availability Codes

Dist	Avail and/or special
A	

2. EXPERIMENTAL TECHNIQUE

Rayleigh Scattering

Rayleigh scattering in gases results from the inhomogeneous nature of the medium produced by fluctuations in the dielectric constant. The Rayleigh scattering intensity is related to the gas density by

$$I_R = C \ I_o \ N \sum_i X_i \ \sigma_{Ri} \tag{1}$$

where I_R is the intensity of Rayleigh scattered light, C a calibration constant of the optics, I_o the incident laser light intensity, N the total molecular number density, X_i the mole fraction of chemical species and σ_{Ri} the Rayleigh cross-section for the ith species. The above expression (1) indicates I_R to depend on the degree of reaction through species-dependent terms. A study of this effect for typical combustion cases (Namer et al., 1980) has shown that Rayleigh scattering can be corrected to provide accurate density measurements (This study is cited as Appendix B). Rayleigh scattering, first used as a diagnostic for density in laminar flows (Robben et al., 1977), has now been extended by the present results for use in studies of turbulent flame propagation. These results will be discussed in section 3.

The optical system for Rayleigh scattering is shown in Figure 2.1. A Spectra Physics 4-watt Argon ion laser is used as the light source for both the Rayleigh scattering and LDA measurements. The laser beam is focussed to 40 micron waist diameter by two lenses and the scattering is collected at 90° from the beam direction by an f/1.2, 55 mm focal length camera lens. The beam passes through a 50 micron slit, is collimated,

and then filtered by a 1.0 nm band-pass filter centered at 488 nm. The
beam is then refocussed to the surface of a RCA 931A type photomultiplier.
The photomultiplier output is amplified by an electrometer with a band-
pass of approximately 1.8 KHz.

Laser Doppler Anemometry

The LDA system shown in Figure 2.2 is the now commonly employed
intersecting dual-beam type with real fringes (Durst et al., 1976).
An equal path length beam splitter with fixed separation of 5 cm is
used, and the two laser beams are focussed by a 250 mm focal length
lens to form the scattering volume. Seed particles are generated by a
cyclone-seeder using nominally 0.3 micron Al_2O_3 particles. Scattering
bursts from the particles are collected at 45° from the forward scatter-
ing direction by a lens, filter and photomultiplier assembly and the
Doppler frequency is obtained using a TSI 1090 frequency tracker.

Computerized Data Acquisition

To facilitate the use of the above optical systems a computerized
data acquisition system based upon a Digital Equipment Corporation (DEC)
PDP 11/10 has been developed, Figure 2.3. The computer system is
operated under DEC RT-11 using an RK05 disk with 1.25 million (16 bit)
words and two IBM 724 magnetic tape drives. The operating system is
accessed by a Tektronix 4025 terminal with graphics display capable of
plotting processes data and a high speed line printer is used for per-
manent page plots and data output listing.

The experimental apparatus is mounted on a three-axis traverse

operated by separate stepping motors which are computer-controlled and thus the flow field positions for Rayleigh scattering and LDA measurements can be scanned automatically.

Measurements are obtained using an 8-channel, 12 bit A/D converter. Samples may be acquired at a constant sampling rate through clock control or individual samples may be initiated by a separate interrupt input by the user. In the latter mode, the time between samples is continuously monitored by the clock. Raw data may be stored in disk memory files or on a 7-track magnetic tape for post-processing with either the PDP 11/10 or the Lawrence Berkeley Laboratory 7600. Details of the data reduction techniques will be discussed below.

3. FLAME PROPAGATION IN GRID-INDUCED TURBULENCE

Experimental Apparatus

In Figure 3.1 a schematic is shown of the experimental apparatus. A coaxial jet is used in which the premixed gases of ethylene and air flow through the central jet. The diameter of the nozzle at the exit of the inner jet is 5.1 cm. An outer coaxial jet with a diameter of 10.2 cm was used to shield the inner flow from mixing with the stagnant surroundings. The flow velocity of the inner and outer jets were matched using the output of a calibrated DISA hot-wire 55P11 and 55D01 anemometer system. The flow rates were also monitored using standard rotameters.

A bi-plane, circular grid was placed 5 cm upstream of the exit of the coaxial jet to generate turbulence. For all conditions described below, the mesh size of the grid, M, was 0.5 cm and the grid elements were 0.1 cm in diameter. A V-shaped flame was stabilized on a 0.1 cm diameter rod positioned at the exit of the nozzle as shown in Figure 3.1. Note that the x coordinate is parallel to the jet axis and the y-coordinate normal to the jet axis. The coordinate of the flame holder is (in cm) (5,0). In a typical measurement sequence, the experimental apparatus was fixed at a given x location and traversed by computer control in the y-direction to provide profiles of velocity and of Raleigh scattering.

Experimental Conditions

Turbulent flame propagation was studied for three flow velocities, U = 245, 501 and 684 cm/sec, with fuel/air equivalence ratios, ϕ, ranging

from 0.55 to 0.75. For the three velocities the equivalence ratios were adjusted to provide a flame half angle, α, of approximately 25° as measured from the flow centerline. The equivalence ratios for these three cases were respectively 0.55, 0.7 and 0.75. At the highest flow velocity (684 cm/sec), additional measurements were obtained at equivalence ratios of 0.6 and 0.7, which gave flame half angles of approximately 10° and 16° respectively. Table 3.1 summarizes these conditions along with the associated mesh Reynolds number $Re_M = \frac{UM}{\nu}$. In Figure 3.2, a photograph of the flames corresponding to the conditions U = 684 cm/sec, ϕ = 0.6, 0.7, 0.75 is shown.

Data Reduction Techniques

A time series analysis of the Rayleigh scattering and LDA data was performed in which statistical moments, power spectra, and probability density and autocorrelation functions were calculated. Standard algorithms were used as discussed by Bendat and Piersol (1971). The time series for the Rayleigh scattering and LDA measurement were obtained by recording on disk memory 5000 samples of the analog signals at a constant rate of 4000 samples/second for the conditions corresponding to U = 684 cm/sec. At the lower velocities samples were acquired at a rate of 2000 samples/sec rate. The output of the photomultiplier for Rayleigh scattering was amplified by an electrometer with a corner frequency of 1.8 KHz. The LDA signal obtained from the TSI 1090 frequency tracker was filtered with an RC filter, with corner frequencies of 2 KHz or 1 KHz depending on whether the sampling rate was 4000 or 2000 samples/sec.

In order to consider the output of the frequency tracker as a continuous signal, it was necessary to have sufficient particles in the flow to provide the tracker with a large number of realizations/second as compared with the highest frequency fluctuation in the flow. With an exit nozzle velocity of 245 cm/sec, the number of realizations per second was typically greater than 5000. At the higher velocities, the number was greater than 20000. At such high data rates, it can be assumed that tracker output is essentially analogous to that of a hot wire signal. Inspection of calculated power spectra confirms this point.

To determine the turbulence fluctuation intensities of Rayleigh scattering and velocity measurements, electronic noise associated with the photomultiplier and frequency tracker must be removed. In the case of Rayleigh scattering, the variance of the noise of the photomultiplier is proportional to the mean current (Robben, 1975). Therefore at the beginning of each profile, photomultiplier fluctuations in the free stream outside the flame were recorded. Since no density fluctuations exists at this location, the signal variance is due primarily to photo-multiplier noise. Then at other locations this variance, adjusted for change in the mean current level of the photomultiplier, is subtracted from the total signal variance. In addition to this error, the mean signal level related to Rayleigh scattering may be contaminated with unrelated background light picked up by the collection optics. This background intensity was measured by moving the collection optics ± 0.38 mm in order to allow the slit to block light scattered directly from the laser beam. The electrometer output measured in this manner was subtracted from the total mean signal. The resultant output is then proportional to the Rayleigh scattering.

The noise associated with the LDA frequency tracker arises from several sources: photomultiplier noise, tracker broadening, and general instrumentation noise. The noise variance was determined by measuring the velocity variance in a laminar jet, i.e. a flow in which the turbulence intensity was approximately 0.5%. The noise level measured in this manner corresponded to a velocity variance of 14.6 $(cm/sec)^2$. This level, which was subtracted from the total variance, is typically less than 10% of the total variance measured under turbulence conditions in which U = 684 cm/sec or 501 cm/sec. At the lower velocity, U = 245 cm/sec, this level is approximately 15% of the variance. Comparison of results for grid-turbulence without combustion (see the following section) and previously reported results indicate that this technique of noise removal is adequate.

Grid-Generated Turbulence

One of the classical problems in fluid mechanics is that of grid-generated turbulence. The problem is attractive since many of the general features of turbulence are exhibited, while the flow description is simplified in that the turbulence may be approximated as isotropic. As a consequence of isotropy the equation for turbulent kinetic energy may be written:

$$\frac{d(\overline{u'^2})}{dt} = -10 \ \nu \ \overline{\left(\frac{\partial u'}{\partial x}\right)^2} \tag{1}$$

where ν is the kinematic viscosity and $\overline{u'^2}$ the averaged square of the fluctuating component of velocity.

Batchelor and Townsend (1948) showed experimentally that $\overline{U}^2/\overline{u'^2}$ is proportional to x/M. This result is independent of U for similar grids apart from small random changes in the virtual origin of turbulence occurring for different mesh Reynolds number $Re_M = UM/\nu$.

The Taylor microscale, λ, an approximate length scale for dissipation is defined by the equation:

$$\overline{\left(\frac{\partial u'}{\partial x}\right)^2} = \frac{\overline{u'^2}}{\lambda^2} \quad . \tag{2}$$

Two consequences of equation (1) and the linearity of $\overline{U}^2/\overline{u'^2}$ with x/M result, namely

$$\lambda^2 \propto \frac{10\nu}{U}$$

and
$$Re_\lambda = \frac{\sqrt{\overline{u'^2}}\,\lambda}{\nu} = const \text{ (independent of x for a given } R_M).$$

These results have been tested by Batchelor and Townsend over the range, $600 < Re_M < 4.4\times10^4$ and $25 < x/M < 150$. In Figure 3.3, $\overline{U}^2/\overline{u'^2}$ is plotted versus x/M for the three inlet velocities of this study. At a given location x/M, $\overline{U}^2/\overline{u'^2}$ is calculated from the data of 20 points spaced at 1 mm intervals across the center of the grid. As predicted for isotropic turbulence, the slopes are approximately constant. As with the data of Batchelor and Townsend (1948), no systematic shift in the origin of turbulence is apparent with changing flow velocity. Hence the result appears to be quite insensitive to slight changes in inlet conditions.

The slope of the curve in Figure 3.3 is 92. The data of Batchelor and Townsend (1948) give an average slope of 134. The ratio on the mesh

size M to mesh element diameter, d for their experiment is 5.3 as contrasted with 5.0 for the present study. As noted by Batchelor and Townsend (1948) considerable scatter exists in the literature. Von Kármán (1938) for M/d = 4.76 found the slope to be 99. Thus considering the close proximity of our measurements to the grid, our results seem quite reasonable.

Taylor's hypotheses may be used to calculate λ from equation (2) (see e.g. Bennett and Corrsin (1978)), i.e.

$$\frac{\overline{u'^2}}{\lambda^2} = \frac{1}{\overline{U}^2} \left(\overline{\frac{\partial u'^2}{\partial t}} \right) . \tag{4}$$

Over the relatively narrow range in Re_M and x/M, λ is found to be approximately 0.2 cm. The statistical variation in λ does not allow equation (1) to be tested under ambient conditions. However, as will be discussed below, the large increase in kinematic viscosity behind the flame front cause relatively large increases in length scale that appear to be governed by equation (1).

Andrews et al. (1975) have correlated turbulent flame speeds with Reynolds numbers based upon the Taylor microscale, i.e. $Re_\lambda = \frac{u'\lambda}{\nu}$. For $Re_\lambda < 100$, they suggested a wrinkled laminar flame model was appropriate. Our data covers the range $10 < Re_\lambda < 30$.

Results and Observations of Flame Propagation Studies

Rayleigh scattering measurements for the conditions of Table 3.1 provide data for mean density profiles, flame location, and density fluctuation intensities. A typical profile of the Rayleigh scattering

level and fluctuation intensity level are shown in Figure 3.4. These results correspond to the flow condition, U = 684 cm/sec, ϕ = 0.75, and x = 8.0 cm. The relative level of Rayleigh scattering has been interpreted as the ratio of the local gas density to the gas density in the free stream. Corrections due to changes in species are neglected. (Namer et al. (1980) have calculated the corrections to be approximately 5%.)

The rms fluctuations shown in Figure 3.4 are primarily due to result of random movement of the flame sheet across the probe volume. The maximum turbulence intensity of 33% is typical for all results. The effect of turbulence fluctuations in the density profile is seen most markedly in the increase in mean flame thickness. While the laminar flame thickness is less than 1 mm for these conditions, the flame width here is approximately 4 mm. The flame width was seen to increase with distance x, varying from 3-5 mm. The increase in thickness would appear to result from the extension of the flame front into the field of grid-generated turbulence, see Figure 3.2.

The probability density function (p.d.f.) plotted in Figure 3.5 was calculated from the Rayleigh data for the conditions of maximum turbulent intensity in Figure 3.4. The distribution is highly bimodal. The highest probability densities are for cold reactants and for completely burned products. Since the chemical reaction rates are quite high, the probability of an intermediate state is low. In the p.d.f. this intermediate state is probably overestimated since the response time of the Rayleigh signal is limited by the band-pass of the electrometer. This p.d.f. along with others, however, indicate the p.d.f. model of Libby

and Bray (1977), in which the intermediate state is neglected, may be reasonable for the conditions of our study.

The evolution of the mean velocity, $\overline{U}$, for various flow conditions is shown in Figures 3.6-3.9. In Figures 3.6-3.8, the flame angle has been held constant.

In Figure 3.6, the velocity profiles are presented for an equivalence ratio of $\phi = 0.55$ and an upstream velocity $U = 245$ cm/sec. For a given x, the location of the flame front may be inferred from the increase in velocity due to heat release of the flame. Since the flame angle is 25°, one would expect considerable flow acceleration in the x-direction. Rayleigh scattering indicates that the peak fluctuation intensity occurs slightly beyond the point of initial increase in velocity. For example, at x = 8.0 the density begins to decrease at $y/d = 15$. The reaction zone thickness is 4 mm. The peak in density fluctuation occurs at $y/d = 12$. We note that the most rapid acceleration of the flow occurs in this region. The rate of acceleration of the flow decreases beyond the reaction zone.

The continued acceleration of the flow past $y/d = 7$ results from the streamwise acceleration of the flow behind the flame as cross-stream momentum is converted to streamwise momentum (see section 4). A similar interpretation holds for the other profiles. At $y/d = 0$, x = 7.0 cm, there is a slight decrease in velocity due to the wake of the flame holder. The Reynolds number of the flame holder based upon the viscosity of the hot products behind the flame is approximately 13.

Similar qualitative trends are exhibited in Figures 3.7 and 3.8; however, the effect of the wake is more pronounced due to the increased drag of

the cylinder. The flame holder Reynolds number for these two cases is respectively 20 and 30.

Inspection of Figure 3.8 indicates the existence of two competing processes in determining the flow pattern: 1) acceleration effects due to heat release and flow convergence, and 2) the decelerating effect due to the drag of the flame holder. At the relatively wide flame angle, corresponding to Figures 3.6-3.8, the effect of heat release and flow convergence is dominant. However, for flames at smaller angles to the upstream flow, it would be expected that there would be less acceleration of the flow in the x-direction. In addition, for a given x-location downstream of the flame holder, the mass flux convected through the flame is considerably less for smaller flame angles. Hence convergence effects are also decreased. Interaction with the wake may dominate in this case.

In Figure 3.9, mean profiles of the u velocity component are presented for the condition corresponding to a flame angle of 10° i.e. $U = 684$ cm/sec and $\phi = 0.6$. As expected the effect of the wake of the flame holder is dominant for this condition. No acceleration of the flow due to heat release is visible except at the farthest downstream locations. Rayleigh scattering indicates that for $x = 8.0$ cm, the mean flame position, as indicated by the peak in the fluctuating intensity, is at $y/d = 5.0$. Bray and Libby (1976) in modelling highly oblique flames have assumed that the streamlines remain undeflected through the flame front. This imposes the kinematic condition that the velocity normal to the flame, U_n, is related to the velocity parallel to the flame front by the relation $U_p = U_n/\tan \alpha$, where α is the previously defined

flame angle. The imposition of this condition causes the model to predict a significant Reynolds stress in the flame and an increase in turbulent kinetic energy due to the interaction of this stress with the velocity gradient. The results presented in Figure 3.8 indicate these condition to be invalid for our study since no increase in the u component occurs, although for the flame angle the u component is nearly parallel to the flame. We shall return to this point later in our discussion of turbulent kinetic energy.

The qualitative features of the flow fields described above are further emphasized by the profiles of turbulence intensity. In Figure 3.10, for example, at $x = 8.5$ we see that for $y/d > 15$, the turbulence level is that due to grid-induced turbulence. At the flame front $y/d = 13$, there is a large increase in fluctuation intensity due to the movement of the flame front across the probe volume. As in the case of Rayleigh scattering, this may be seen in terms of the velocity p.d.f. The p.d.f. of velocity is shown in Figure 3.11. As with the density p.d.f. a bimodal distribution occurs, indicating the fluctuation of the flame front. The location of the peaks in velocity fluctuation intensity are found to correlate well with the location of peak density fluctuation. Behind the flame front the turbulence intensity decreases to approximately half of the level upstream of the flame. Thus a substantial decrease in turbulent kinetic energy occurs. This is consistent with the model of Bray and Libby (1976) which suggests that dilatation effects will be dominant in flows propagating at relatively large angles to the upstream flow direction.

In Figure 3.12, profiles of turbulent velocity intensities are

presented for the conditions of an oblique flame, at an angle of 10° to the jet axis. Note again that Rayleigh scattering indicates that mean flame positions for x = 8.0 and 11.0 cm are respectively y/d = 5 and 11. These profiles differ dramatically from those of Figure 3.10. No large increase in intensity at the flame front is expected since no large increase in velocity in the x-direction is induced by the flame (Figure 3.9). The increase in turbulence intensity, at y/d = 3 is similar to that which is found in the wake of a cylinder in isothermal flow. Recall that the flame holder Reynolds number for this case is approximately 30, based upon the viscosity of the hot products.

In order to determine the source of the velocity fluctuations, the power spectrum was calculated from the velocity time series at x = 11, y/d = 5. The results, shown in Figure 3.13, show a peak at approximately 500 Hz. The Strouhal number corresponding to this frequency is 0.07. Roshko (1953) in a study of vortex shedding found that the Strouhal number to be 0.12 for a circular cylinder of Reynolds number 40. In this Reynolds number range, the Strouhal number decreases with decreasing Reynolds number. It seems reasonable to attribute the peak intensities shown in Figure 3.11 to vortex shedding from the flame holder since the frequency range is reasonable and the location of the intensity peaks are uncorrelated with flame position.

The decrease of turbulent velocity intensity at y/d = 10, x = 11.0 further confirms our observation that the undeflected streamline assumption of Bray and Libby (1976) is inappropriate. Since a decrease in turbulent kinetic energy across the flame front is related to flow dilatation effects, it is reasonable to expect that the streamlines are deflected.

Grid-generated turbulence results in a three-dimensional spectrum of length scales. In Figure 3.14 the power spectra upstream of the flame front is presented for the conditions corresponding to U = 684 cm/sec and ϕ = .75. The spectral shape is quite similar to that reported in many studies of grid-generated turbulence. The autocorrelation function, the Fourier transform of the spectral density function, is shown in Figure 3.15. The integral length scale, the scale at which turbulent energy is produced, may be defined as:

$$L = \frac{\overline{U}}{\overline{u'^2}} \int_0^\infty u(t)u(t+\tau)d\tau \ .$$

For the autocorrelation of Figure 3.14 L $\cong$ 6 mm. This is reasonable since the mesh spacing, M = 5 mm. At the flame front, autocorrelation functions suggest that there is a large increase in length scale. These results are difficult to interpret due to the movement of the flame. Behind the flame front, where tracker noise is a higher percentage of the total variance, digital filtering of the time series will be required to calculate the integral scale. We are currently completing a more detailed study of these effects.

In normal grid-generated turbulence, Batchelor and Townsend (1948) have shown theoretically and experimentally that

$$\lambda^2 = \frac{10\nu}{U} (x-x_0)$$

where x_0 is the virtual origin of turbulence. The scale is thus predicted to increase as the turbulent kinetic energy decays with distance x. Behind the flame this increase in scale is substantially enhanced by the

increased viscosity. In Figure 3.16, our results are presented at the location well behind the flame front, $y/d = 5$. The value of U is taken as the average velocity between locations $7 \leqslant \frac{x}{M} \leqslant 18$. Along with the data, a curve of slope $\frac{10\nu}{U} M$ is shown. The good agreement with the data indicates that the turbulence behind the flame decays in a manner similar to isotropic turbulence. An analysis of the microscale near the flame front, as in the case of integral scales, will require more sophisticated analysis due to the movement of the flame front.

Summary

Our study of flame propagation in grid-induced turbulence has indicated that for flame fronts at relatively large angles to the upstream flow, the effect of heat release and flow dilatation is to decrease the turbulent kinetic energy. At smaller angles, the streamlines are deflected in such a manner that dilatation effects are still dominant. These data indicate that the deflection of streamlines of the flame front must be taken into account in order to properly model the turbulent kinetic energy of flames. The effect of drag on the flame holder has also been shown to have a major effect on the flow field behind the flame, particularly at small flame angles. This suggests that results for such conditions are not typical of the interaction of a flame front with grid-induced turbulence. Preliminary results for length scales indicate there may be large increases in integral scales at the flame front. Well behind the flame front the evolution of the integral scales suggests a return to flow dynamics found in grid-induced turbulence.

TABLE 3.1

U	Re_M	Equivalence Ratio ϕ	Flame Half Angle α
684	2280	.75	25
684	2280	.70	16
684	2280	.6	10
501	1670	.7	25
245	817	.55	25

4. INTERACTION OF A FLAME AND A KÁRMÁN VORTEX STREET

Introduction

One of the major shortcomings of models of turbulent flame propagation using the wrinkled laminar flame model is the need to make assumptions about the geometry of the wrinkling. The importance of this problem has been noted by Karlovitz (1954), Scurlock and Grover (1953), Peterson and Emmons (1961), and Clavin and Williams (1979). However, details of the wrinkling process are still not sufficiently understood for accurate numerical models of flame propagation under these circumstances to be developed. In order to advance our understanding of the interaction of turbulent eddies with flame fronts, we have studied the interaction of an otherwise laminar flame with a two-dimensional Kármán vortex street using Rayleigh scattering and LDA. Although this is an idealization of a turbulent flow, many of the important features of turbulent flame propagation are exhibited. Furthermore, the regularity of the vortex street enables us to use phase-locked signal averaging to produce the details of the complete two-dimensional flow field as a function of time. These experiments can supply a critical portion of the data base from which numerical models of turbulent flame propagation may be formulated and tested. Previous measurements (Namer et al., 1977) under Air Force Contract F44628-76-3-0083 demonstrated that Rayleigh scattering along with LDA measurements were capable of yielding data of the necessary quality to construct detailed two-dimensional flow fields as a function of time. In order to ascertain that the velocity field was the desired one, LDA measurements have been performed first and the results are reported here. Rayleigh scattering density field measurements

will be completed shortly and will not be discussed further at this time.

The Kármán Vortex Street

The wake behind a cylinder for Reynolds numbers between 40 and 5000 exhibits a fairly regular pattern of alternately rotating vortices known as a Kármán vortex street. This phenomenon has been studied extensively by many investigators. A stability analysis of an ideal Kármán vortex street, consisting of two staggered infinite parallel rows of vortices whose strengths are equal but opposite in sense (see Figure 4.1), has shown that the only arrangement which exhibits neutral stability is one in which $h/\ell = 0.281$ (e.g. Lamb, 1945). Fage and Johansen (1927) and Rosenhead and Schwabe (1930) measured the variation of the vortex shedding frequency with Reynolds number. Roshko (1953) and Roshko (1954) provide a substantial amount of data on the dependence of the Strouhal number on the Reynolds number. Furthermore, as in Kovasznay (1949), Roshko (1953) found that a stable, regular vortex street is obtained only for Reynolds numbers between 40 and about 150. Various authors quote different values of the upper limit. This may be due to the fact, not generally realized, that for Reynolds numbers near the lower limit the vortex street is not shed from the cylinder but develops from a laminar wake instability (see Kovasznay, 1949). When the Reynolds number increases to some critical value the vortices begin to be shed directly from the cylinder. Tritton (1959) and Marris (1964) suggest that this critical value of Reynolds number is about 90. During this study this transition was observed at various Reynolds numbers down to 75. The data of Roshko (1953) suggests that he may have observed this phenomenon at a Reynolds number of 150, although not remarking on it.

Operating Conditions and Experimental Apparatus

Considerations of the above criteria and the laminar flame propagation speed, stability, and the physical dimensions of the experimental facility defined the constraints and the range of operating conditions. For instance, two cylinders were used to generate the vortex street at different frequencies. Their diameters were necessarily small (2.0 and 3.0 mm) in order to maintain large length-diameter ratios needed to obtain an essentially two-dimensional flow field and yet large enough to accommodate the reference hot wire. The Reynolds number requirements for stable vortex shedding established the "free stream" velocity, U_∞, at 55 cm/sec. Thus the Reynolds numbers were 73 and 110 for the 2.0 and 3.0 mm rods respectively. In order to get stable flame propagation and avoid flashback or blowoff an equivalence ratio of 0.52 was chosen for the premixed C_2H_4-air flames studied. Furthermore, the cylinder had to be placed far upstream of the flame in order to prevent the flame from attaching itself to the vortex generating cylinder. This precaution was quite important since the reference hot wire necessary for phase-locked measurements would be destroyed by the flame if flashback occurred. The coordinate system and the locations, in mm, of the flame holder and vortex generating cylinder are shown in Figure 4.2.

Due to the operating conditions described, conventional hot wire probes could not be used because conventional probe holders, being comparable in size to the vortex generating cylinder, would perturb the flame in a similar manner. A novel hot wire probe was designed and constructed which incorporates the cylinder as both a vortex street generator and hot wire probe holder. A schematic of the construction is

shown in Figure 4.3 and a top view of the test section is shown in Figure 4.4. The vortex generating cylinders used were pyrex tubes. The wire sensor, 0.02 mm diameter gold plated tungsten, was spot welded to the tips of 0.5 mm diameter platinum wire supports 10 mm apart. The sensor position is fixed at 10 mm above the cylinder and offset to the side by about one cylinder radius. In this position the signal from the sensor was a maximum.

The hot-wire, described above, supplied the reference signal for the phase-locked averaging. The reference signal was sampled simultaneously along with the LDA tracker output voltage at a 1 KHz rate on two channels of the A/D converter and the data was stored in a file (see chapter 2). 4070 samples were taken at each location of a two-dimensional x-y grid. For comparison, measurements of the wake with no combustion were made utilizing 2022 samples per channel per location.

Ensemble Averaging Technique

The feature which makes this study attractive is the regularity and the repetitive nature of the Kármán vortex street in the wake of a cylinder. Phase-locked or ensemble averaging is possible and highly resolved velocity and density fields can be found as a function of time or phase. The ensemble average is obtained by averaging measurements at the same location and phase. Thus, for example, the velocity measurements are reduced from $u(x,y,t)$ to $\tilde{u}(x,y,\phi)$ and the density measurements can be reduced from $\rho(x,y,t)$ to $\tilde{\rho}(x,y,\phi)$, where ϕ here is the phase angle of the flow field.

The basis for ensemble averaging is the reference hot wire signal which can be used to establish the phase of the flow field. The method

whereby this was carried out for this experiments is described in the following. Consider a function, $g(t)$, which may represent an oscillating velocity or density as a function of time at a given location, and which is sampled at discrete times to generate a set of measurements $g(t_i)$. Further consider a reference function $R(t)$, where $R(t)$ is periodic with mean $\overline{R(t)} = 0$. There will be N roots or zero crossings t_n^o, $n=1, \ldots N$, which satisfy $R(t_n^o) = 0$ with $\frac{dR}{dt}(t_n^o) > 0$. Therefore, there are N-1 complete cycles whose periods are defined by $T_n = (t_{n+1}^o - t_n^o)$. The phase associated with a measurement $g(t_i)$ is defined by $\phi_i = (t_i - t_n^o)/T_n$, where $t_n^o < t_i \leq t_{n+1}^o$ and $0 < \phi_i \leq 1.0$. Thus $g(t_i)$ can be replaced by $g_n(\phi_i)$. The ensemble average is thus calculated for 20 equally spaced values of the phase angle ϕ_j, $j = 1,20$, from

$$\tilde{g}(\phi_j) = \sum_{n=1}^{N-1} g_n(\phi_i)$$

with $\phi_j - 0.025 < \phi_i \leq \phi_j + 0.025$. The number of samples averaged at each phase angle may be estimated by dividing the total number of samples by 20.

In order to insure that there were no significant irregularities in the vortex street, data is only considered when the cycle period, T_n, is within 10% of the average period, TAU. In general the amount of data rejected by this criteria was small.

$\tilde{g}(\phi_j)$ can be smoothed further by a truncated Fourier series (e.g. Kovasznay, 1949) by defining

$$\hat{g}(\phi) = \sum_{m=0}^{2} \{A_m \cos(2\pi m\phi) + B_m \sin(2\pi m\phi)\}$$

where
$$A_m = 2 \sum_{j=1}^{20} \tilde{g}(\Phi_j) \cos(2\pi m \Phi_j) \delta \Phi_j$$

$$B_m = 2 \sum_{j=1}^{20} \tilde{g}(\Phi_j) \sin(2\pi m \Phi_j) \delta \Phi_j$$

and $\delta \Phi_j = 0.05$

With such an averaging technique at every point on a two-dimensional x-y grid such quantities as $\hat{u}(x,y,\Phi)$ and $\hat{\rho}(x,y,\Phi)$ may be found. A convenient way to present these are by plotting lines of constant $\hat{u}$ or $\hat{\rho}$ for various values of Φ, thus reproducing a series of detailed "snapshots" of the entire flow field.

Results and Discussion

The streamwise velocity component, u, was measured at points on a two-dimensional x-y grid using LDA for three cases: a) in the wake of a 2.0 mm cylinder, b) through a flame in the wake of a 2.0 mm cylinder, and c) through a flame in the wake of a 3.0 mm cylinder. Presented here are the mean and standard deviation (rms) of N along with contour plots of the smoothed ensemble averaged velocity field.

In order to know what an ideal vortex street would look like when represented by contours of u, contours were computed for the ideal vortex street in Figure 4.5(a) and are shown in Figure 4.5(b). It can be seen that each vortex is represented by a paired structure consisting of a high and a low velocity center. This is because the vortex retards the flow in the center of the street and augments it on the outside. Figure 4.6 shows the wake of a 2 mm cylinder at four phase angles,

$\Phi \equiv T/TAU$. The vortex shedding frequency was 34 Hz and the convection velocity of the vortices was 50 cm/sec. Clearly the phase-locked averaging technique is quite capable of reproducing the two-dimensional flow field as a function of the phase angle. Figure 4.7 shows a typical profile of the mean and rms of u across the wake. This agrees well with Kovasznay (1949) and Roshko (1953). For only this figure the vortex generating cylinder is located at coordinates $(x,y) = (-25.0,0.0)$. Otherwise the coordinate system is as defined in Figure 4.2 and the vortex generating cylinder is at $(x,y) = (-25.0,12.5)$.

Typical mean and rms velocity profiles across a flame in the wake of 2.0 and 3.0 mm cylinders are shown in Figure 4.8. The key features to note here are the deflection of the wake by the flame, the large rms velocity found at the flame, and the continued acceleration of the flow behind the flame. The level of velocity fluctuations at the flame and, in fact, throughout the flow field are not significantly different for the two cases. A series of mean velocity profiles at various streamwise locations are shown in Figure 4.9.

The deflection of the flow, and hence the wake, is due to the small pressure drop across the flame which is necessary for the flow to accelerate when the density falls due to combustion heat release. This, we believe, is an important effect of combustion heat release on the flow field upstream of the flame, which in turn will affect the manner in which the combustion wave behaves. It is important that models which propose to predict realistically the combustion process account for this phenomenon. Neglecting this phenomenon may lead to incorrect conclusions such as the concept of flame generated turbulence (see Karlovitz, 1954, and Richmond et al., 1960) or incorrect values of the flame speed (see Smith and Gouldin, 1977).

The large value for the rms velocity at the flame is due to an Eulerian effect when the flame fluctuates across the probe volume. This should in no way be construed as flame generated turbulence. In fact, for these studies, the combined effect of dilatation, due to the acceleration of the flow normal to the flame, and the increase in the viscosity, due to the increase in temperature, will tend to dissipate and reduce any turbulent kinetic energy in the flow.

When the flow is accelerated across a flame, the acceleration is in the direction normal to the flame. For the type of flames studied here, this implies a fairly strong acceleration in the cross-stream velocity component. If the axis $y = 0$ may be considered to be an axis of symmetry across which no flow can pass, the cross-flow must be diverted parallel to the x-axis (in a similar fashion to stagnation flow) and a further acceleration behind the flame is observed. These features are further illustrated in Figure 4.10 which shows contour plots of the mean stream-wise velocity component for the two cases.

A series of "snapshots" of the flow field are shown in Figures 4.11 and 4.12 for the flame in the wake of a 2.0 and 3.0 mm rod respectively. These consist of constant velocity contours at a given phase angle as obtained from the phase-locked averaging. TAU, the average period, is equal to the reciprocal of the vortex shedding frequency. The shedding frequencies are 32 and 24 Hz, respectively, for the two figures. The flame location or shape is not clearly defined in these pictures because of the manner which the flow accelerates behind the flame does not lead to a clear interface between reactants and products. It remains for Rayleigh scattering measurements to more accurately define the wrinkling of the flame. However, one may consider the properties of a particular

contour level, say 74 cm/sec, to be, at least qualitatively, representative of the flame. Some features become immediately apparent. The fluctuations of the flame in the wake of a 2.0 mm rod do not appear to be as pronounced as those in the wake of a 3.0 mm rod. This correlates well with Markstein (1959) who shows that for this range of frequency of disturbance most flames will be more stable to disturbances at 32 than 24 Hz. However, the acceleration through the flame is greater for the former case. This may be due to weaker and smaller vortices shed from the 2.0 mm cylinder. This explains why the rms level at the flame for the two cases are comparable (see Figure 4.8). The vortex structure observed in Figures 4.5(b) and 4.6 as well as upstream of the flame are not observed behind the flame. There are a number of reasons for this. First, since the streamwise component of the flow continues to accelerate behind the flame, local highs or lows will not be observed. Second, because of the need to choose larger contour intervals behind the flame in order to get reasonable plots the resolution in velocity is greatly reduced compared to what it is upstream of the flame. Finally, there is an indication, from the data, that the strength of the vortices are reduced behind the flame. However, further analysis is necessary to substantiate this.

Summary

The study of the interaction of a Kármán vortex street and a flame, although an idealized flow, has resulted in a better understanding of the turbulent combustion process. The regularity of the vortex street makes phase-locked averaging feasible. We have made and will continue to make detailed time-resolved density and velocity measurements, using Rayleigh scattering and LDA respectively. Two key results were obtained

from this study. First, it is clear that models which hope to predict combustion flows must account for combustion heat release and its affect on the flow upstream and downstream of the flame. Second, the tendencies of flame stability described by Markstein (1959) were demonstreated here. The dependence of flame distortion and wrinkling on the frequencies (and by implication, the phase relations) of the incident flow fluctuations should also be accounted for in models of turbulent combustion. Further, implied by this study is that dilatation and increased viscosity, both due to the combustion heat release, may cause the strength of the vortices to decrease and the fluctuations to decay very quickly behind the flame.

REFERENCES

Andrews, G. E., Bradley, D. and Lwakabamba, S. B., Combustion and Flame, 24, 285 (1975).

Batchelor, G. K. and Townsend, A., Proc. Roy. Soc., A, 193, 539 (1948).

Bendat, J. S. and Piersol, A. C., Measurement and Analysis of Random Data, Wiley, New York (1971).

Bennett, J. C. and Corrsin, S., Phys. Fluids, 21, 2129 (1978).

Bray, K.N.C. and Libby, P., Phys. Fluids, 19, 1687 (1976).

Cheng, R. K., Bill, R. G., Jr., Robben, F., Schefer, R. and Talbot, L., Paper presented at 2nd Int. Symposium on shear layers, Imperial College, U.K. (1979).

Cheng, R. K., Bill, R. G., Jr. and Robben, F., to appear 18th Symposium (Int.) on Combustion.

Chorin, A.J., "Numerical Study of a Slightly Viscous Flow," J. Fluid Mech., 57, 785 (1973).

Clavin, P. and Williams, F. A., J. Fluid Mech., 90, 589 (1979).

Clavin, P. and Williams, F. A., J. Fluid Mech., 90, 3 (1979).

Damkohler, G. Z., Elektrochon, 46, 601 (1940); English translation, NACA Tech. Memo, 1112 (1947).

Durst, F., Melling, A. and Whitelaw, J. H., Principles and Practice of Laser Doppler Anemometry, Academic Press, New York, 405 (1976).

Fage, A. and Johansen, F. C., Proc. Roy. Soc. A, 1116 (1927).

Karasalo, I., Chorin, A. J., Namer, I., Robben, F., Talbot, L., "Numerical Simulation of the Interaction of a Flame with a Kármán Vortex Street," LBL-10679, Lawrence Berkeley Laboratory Report (1980).

Karlovitz, B., "Selected Combust. Probs," Butterworths, London, 248 (1954).

Kovasznay, L.S.G., Proc. Roy. Soc. Lon. A, 198 (1949).

Lamb, H., "Hydrodynamics," Dover, pp. 224-229 (1945).

Libby, P. A. and Bray, K.N.C., AIAAJ, 15, 1186 (1977).

Markstein, G. H., J. Aero. Sci., 18 (1951).

Marris, A. W., J. Basic Engineering, 86 (1964).

Namer, I., Agrawal, Y., Cheng, R. K., Robben, F., Schefer, R. and Talbot, L., UCB Report FM-77-3 (1977).

Namer, I., Schefer, R. W. and Chan, M., LBL-10655, Lawrence Berkeley Laboratory Report (1980).

Peterson, R. E. and Emmons, H. W., Phys. of Fluids, 4 (1961).

Richmond, J. K., Grumer, J. and Burgess, D. S., 7th Symposium (Int.) Combust., 615-620 (1960).

Robben, F., LBL-3294, Lawrence Berkeley Laboratory Report (1975).

Rosenhead, L. and Schwabe, M., Proc. Roy. Soc. A, 129 (1930).

Roshko, A., NACA TN 2913 (1953).

Roshko, A., NACA TN 3169 (1954).

Schefer, R. and Robben, F., LBL-9684, Lawrence Berkeley Laboratory Report (1979), also to appear in Combustion and Flame .

Scurlock, A. C. and Grover, J. H., 4th Symposium (Int.) on Combustion (1953).

Smith, K. O. and Gouldin, F. C., Paper No. 77-183, presented at AIAA 15th Aerospace Sciences Meeting, Los Angeles, California (1977).

Spalding, D. B., Combustion and Flames, 1, 287 (1957).

Talbot, L., Cheng, R. K., Schefer, K. W. and Willis, D. R., LBL-10113, Lawrence Berkeley Laboratory Report (1980).

Tritton, D. J., J. Fluid Mech. 6 (1959).

OPTICS FOR RAYLEIGH SCATTERING
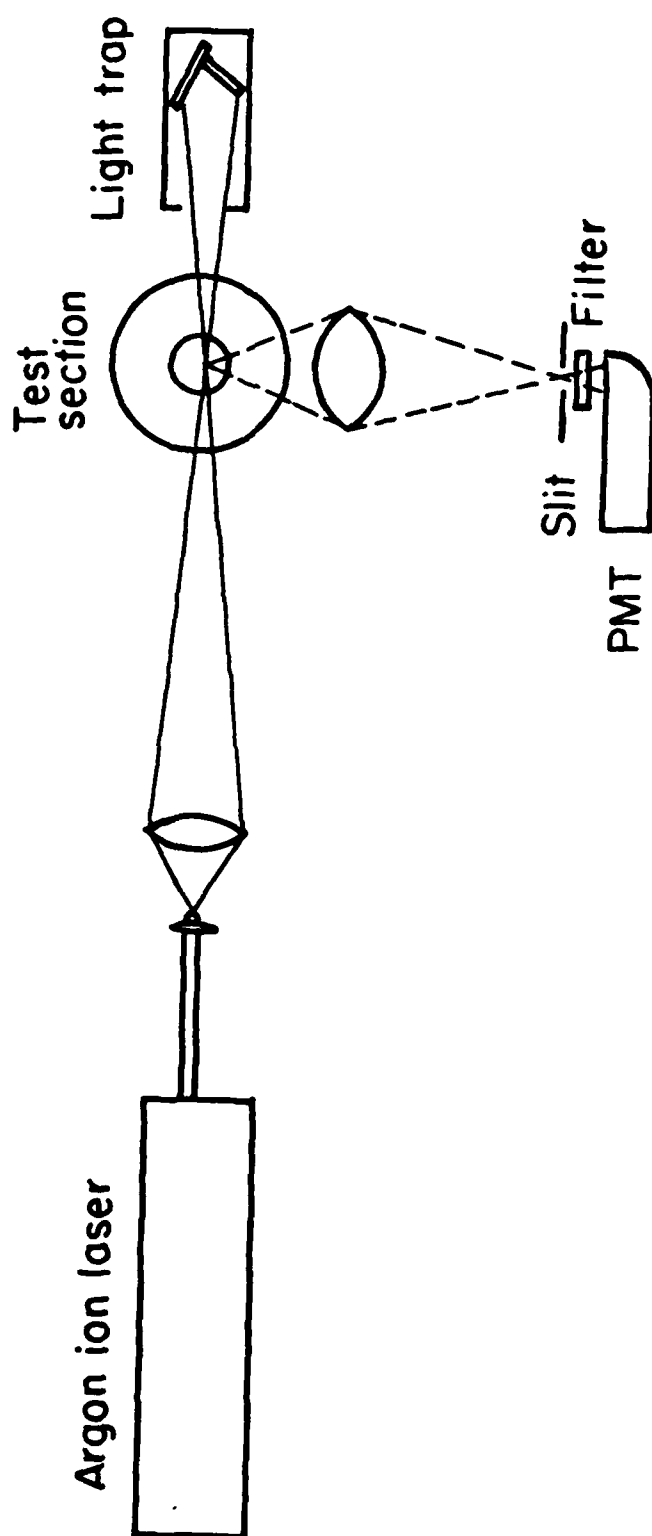
Figure 2.1

XBL803-3178

Optics for Laser Doppler Velocimeter
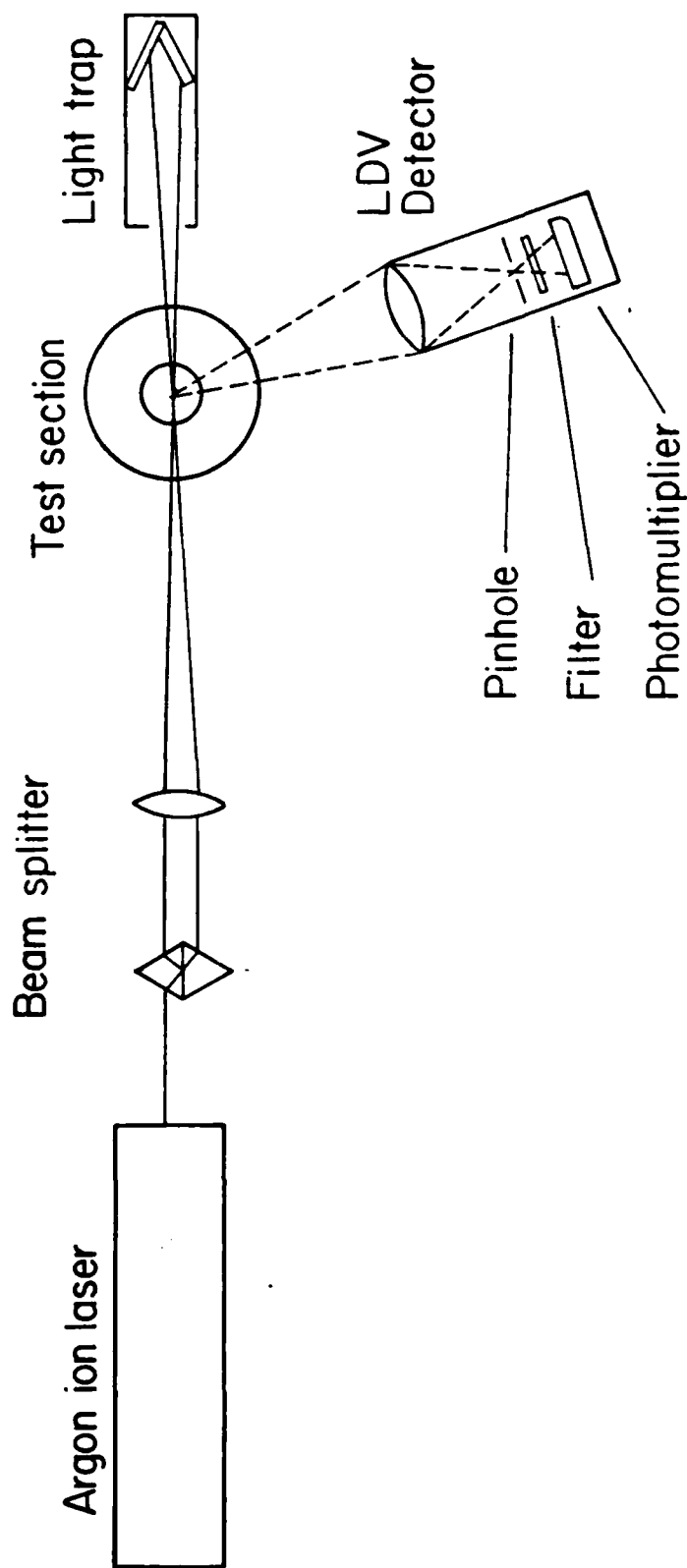
Figure 2.2
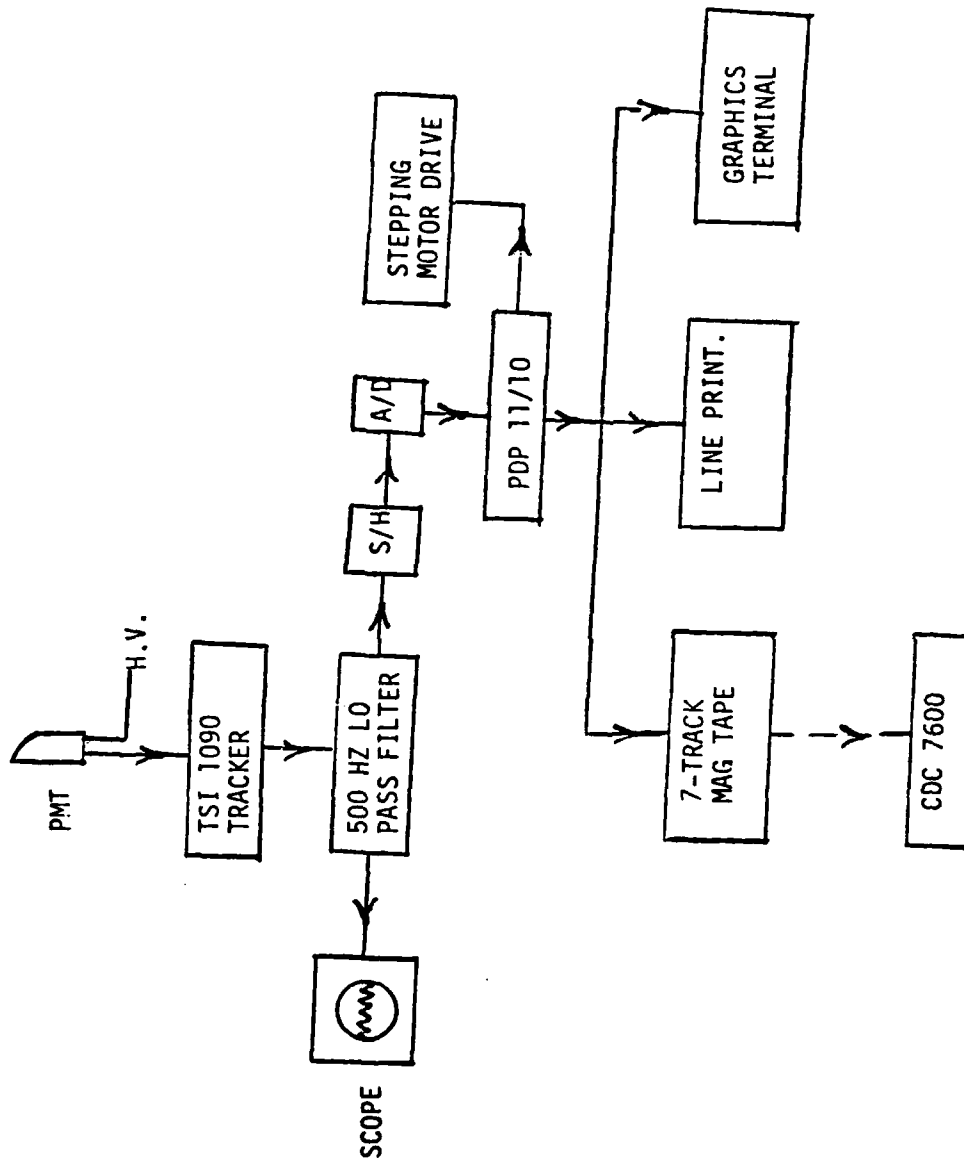
XBL 804-4130

SCHEMATIC OF LDV DATA ACQUISITION SYSTEM

Figure 2.3

Flame Propagation in Grid Induced Turbulence
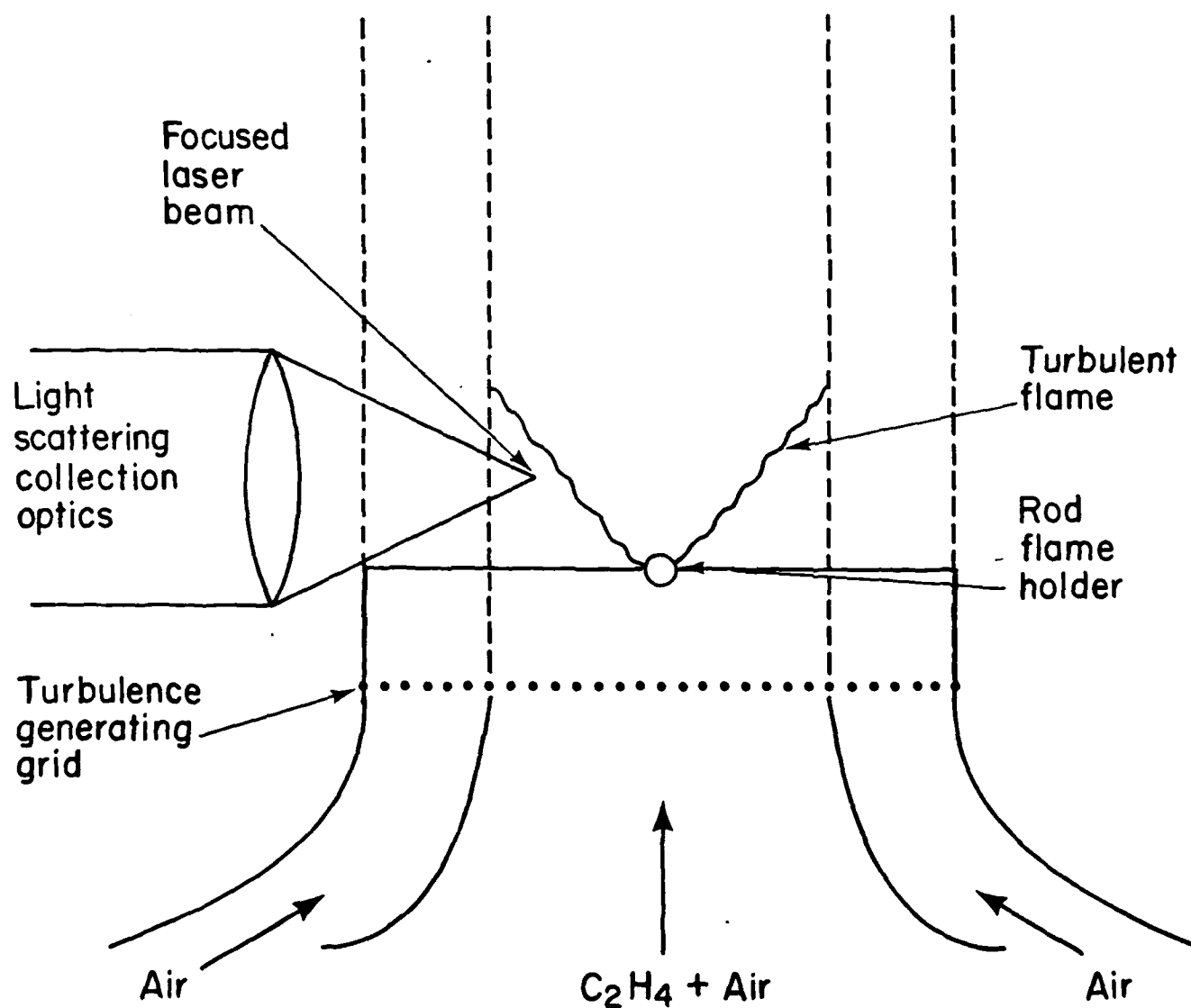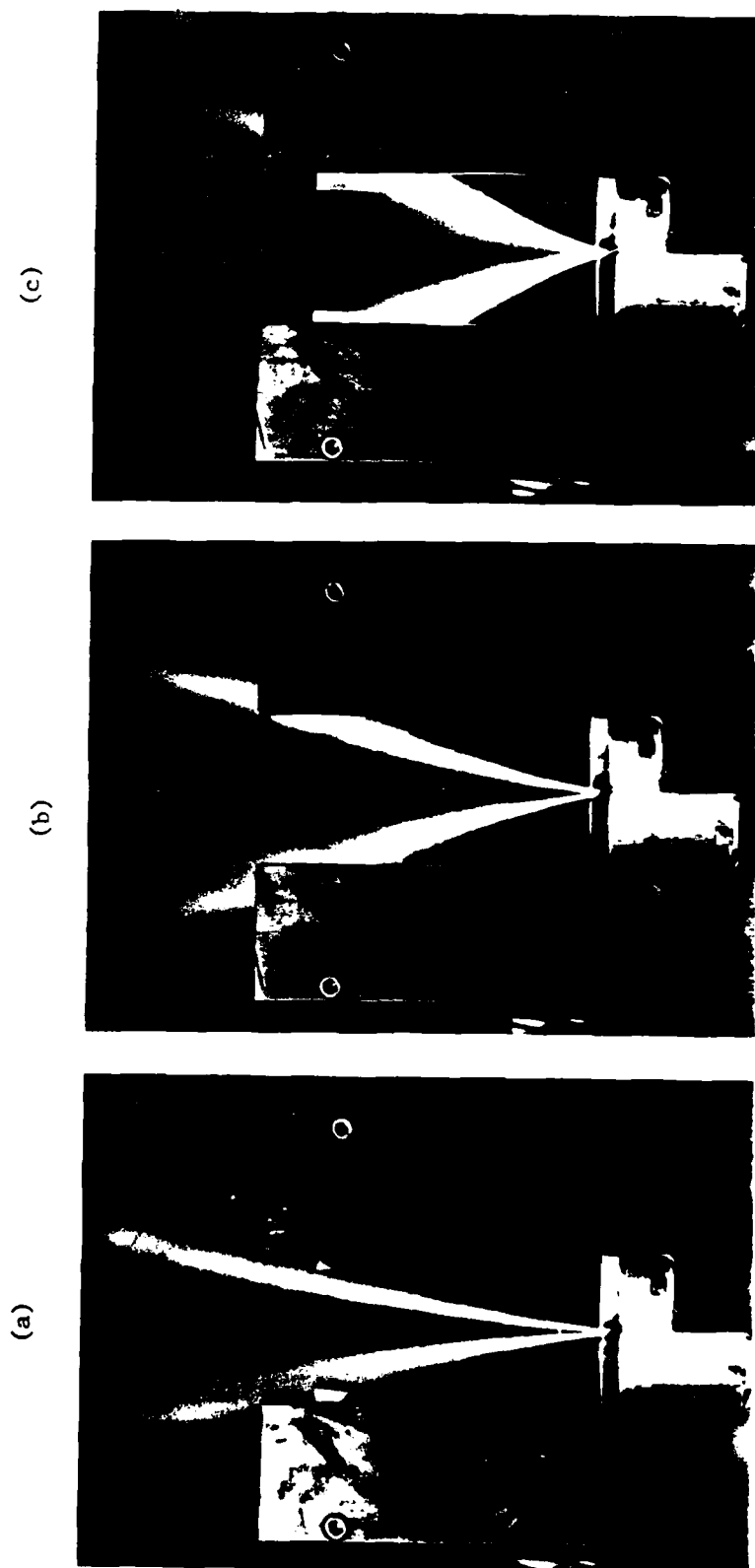
Figure 3.1

Figure 3.2 - Flame propogation in grid induced turbulence: U=684 cm/s.
(a) ϕ = 0.6, (b) ϕ = 0.7, (c) ϕ = 0.7 .
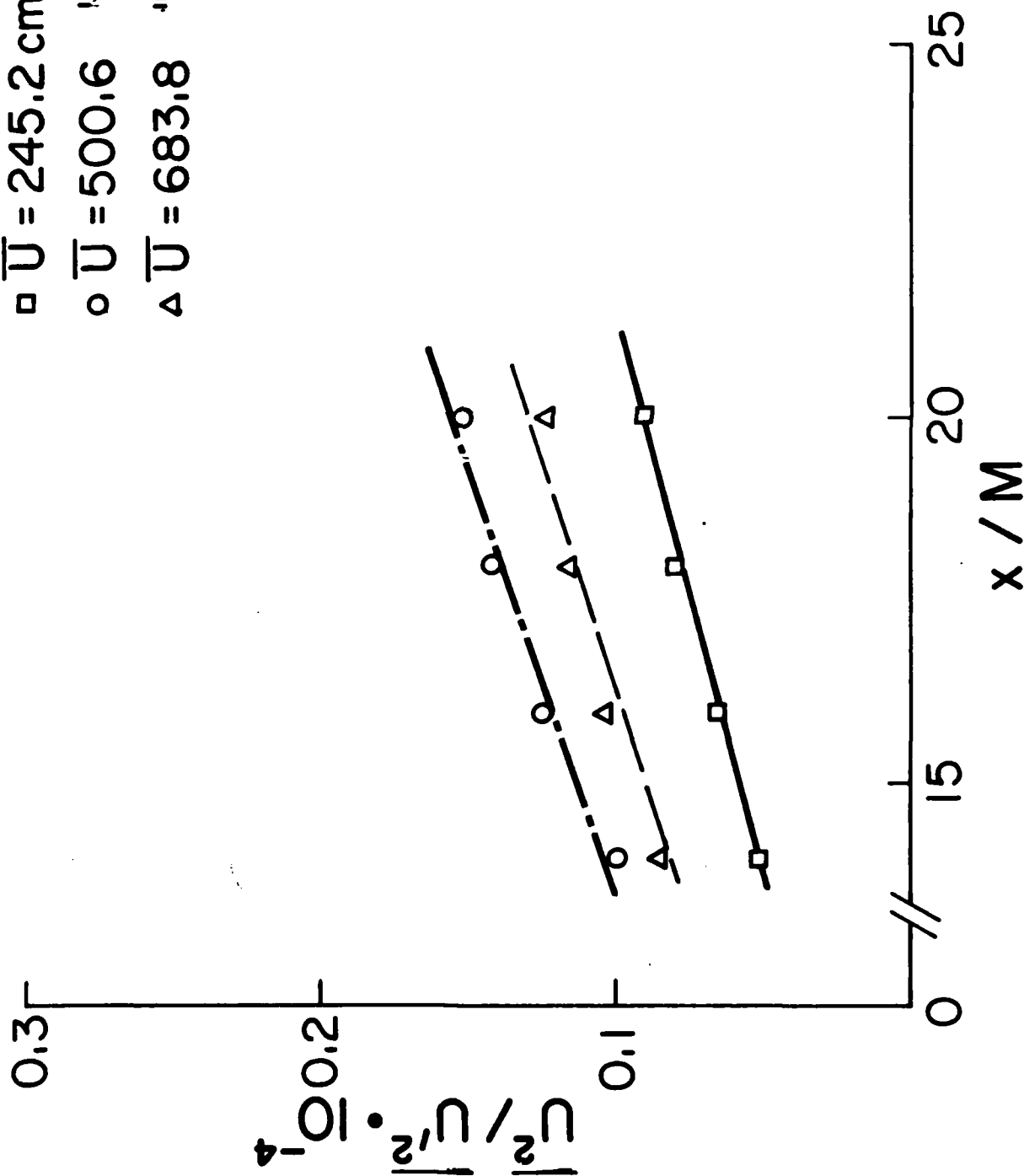
Figure 3.3 EVOLUTION OF GRID-GENERATED
TURBULENCE

XBL 802-369
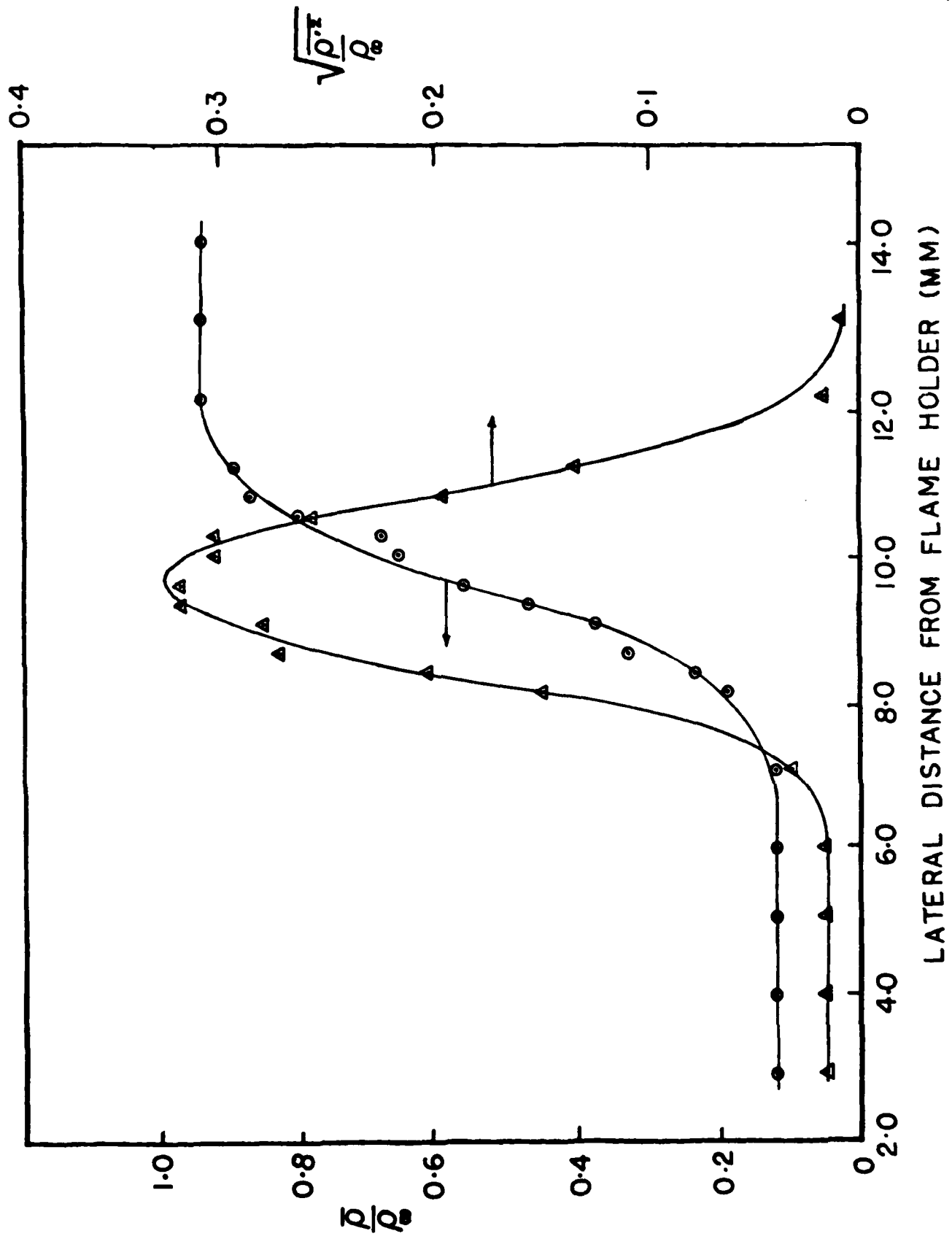
Figure 3.4 MEAN AND RMS INTENSITY PROFILES OF DENSITY THROUGH A FLAME
IN GRID-INDUCED TURBULENCE
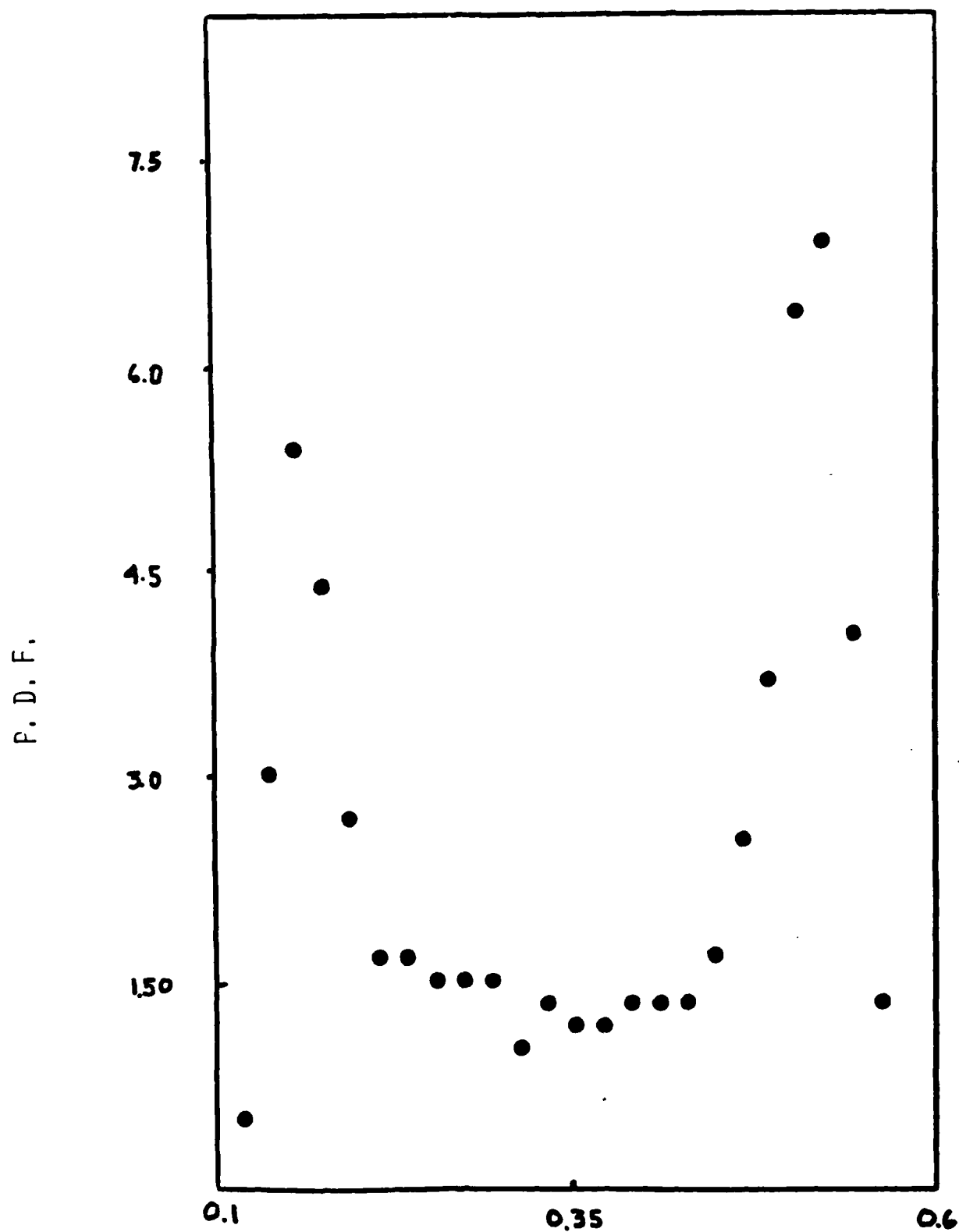
Figure 3.5 PROBABILITY DENSITY FUNCTION OF ELECTROMETER OUTPUT
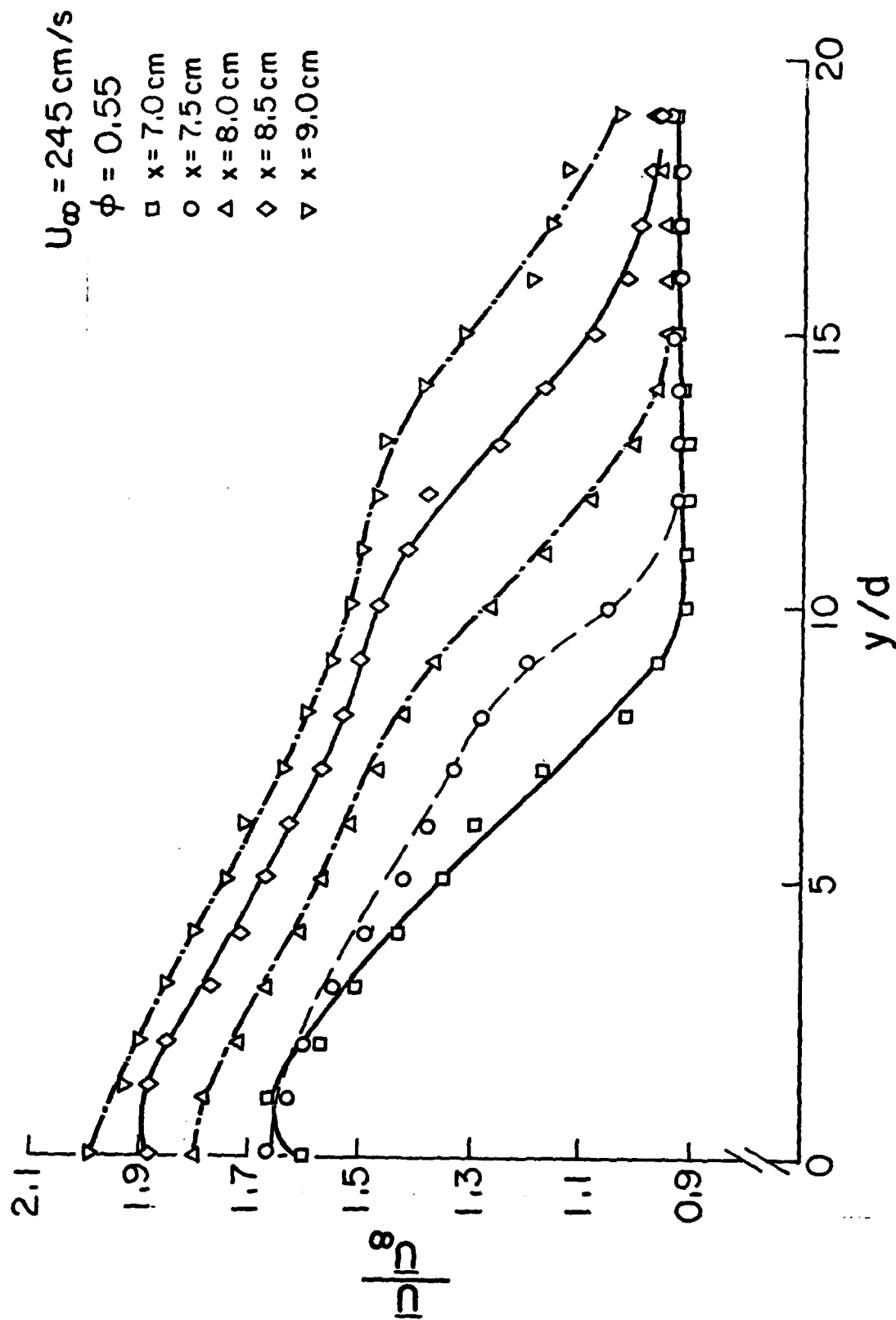
Figure 3.6 MEAN VELOCITY PROFILES THROUGH A FLAME IN GRID-INDUCED TURBULENCE

XBL 802-366
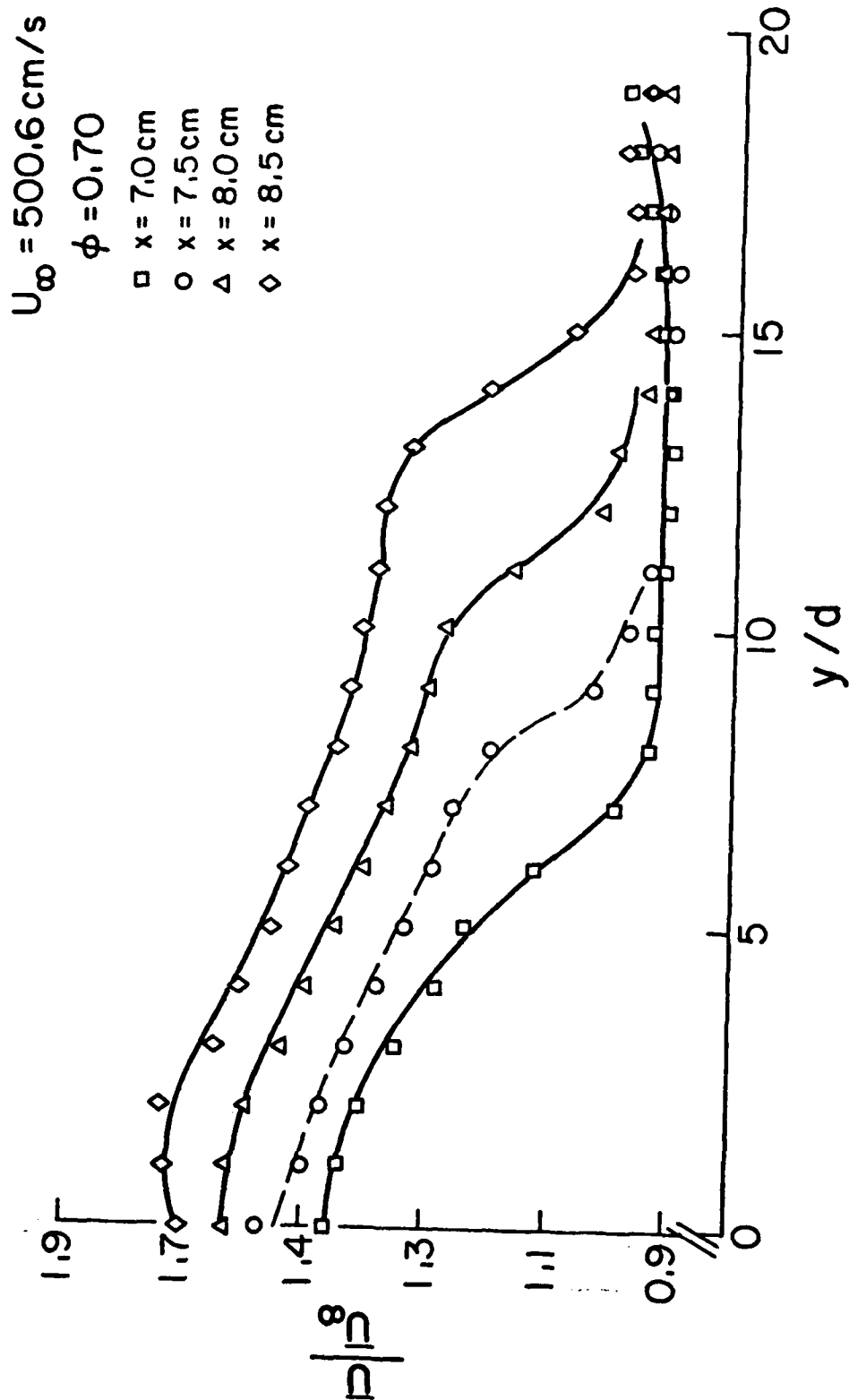
Figure 3.7 MEAN VELOCITY PROFILES THROUGH A FLAME IN GRID-INDUCED TURBULENCE

XBL 802-387
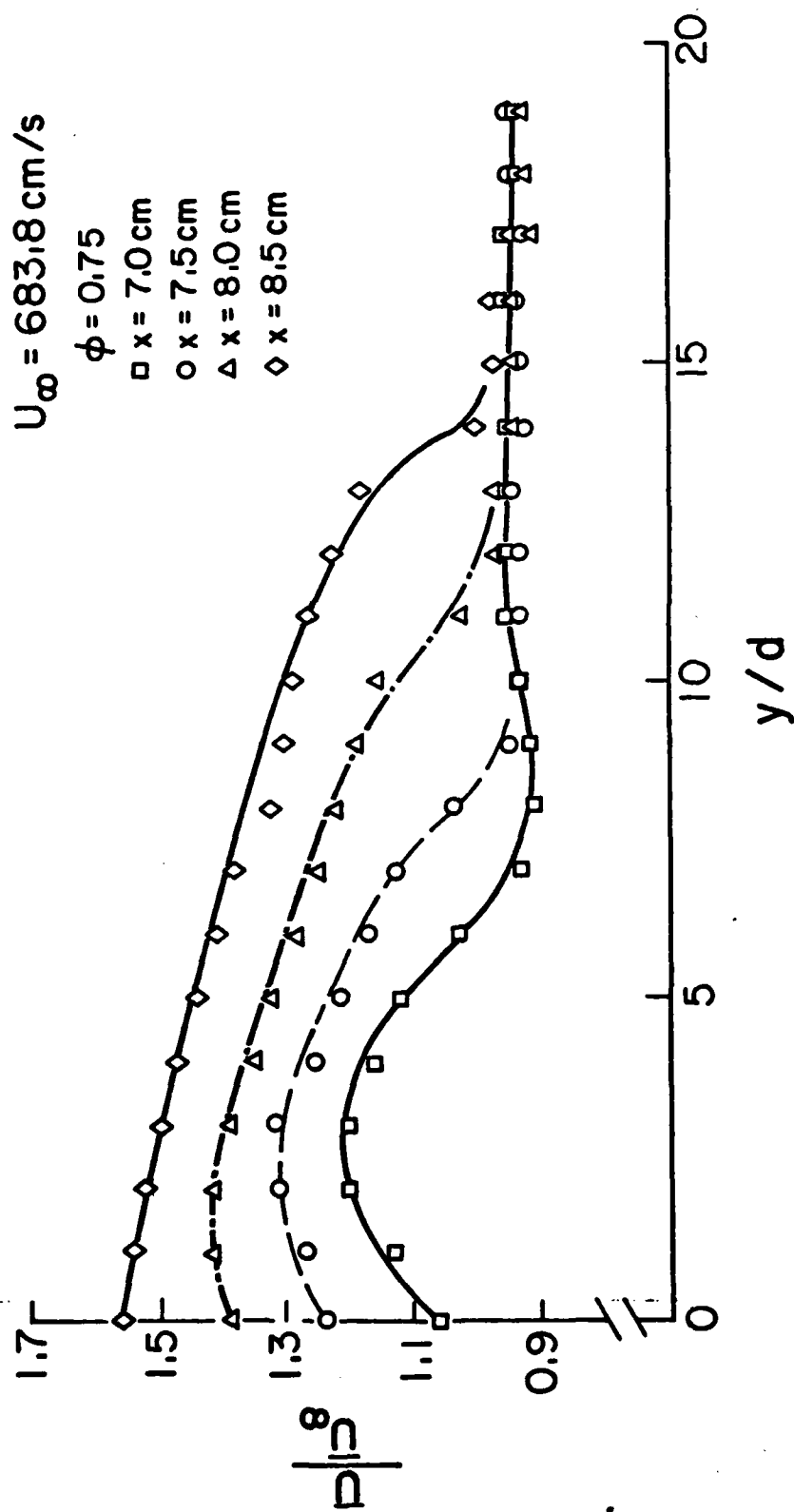
Figure 3.8 MEAN VELOCITY PROFILES THROUGH A FLAME
IN GRID-INDUCED TURBULENCE

XBL 802-368

$U_\infty = 683.8 \, cm/s$

$\phi = 0.75$

□ $x = 7.0 \, cm$
○ $x = 7.5 \, cm$
△ $x = 8.0 \, cm$
◇ $x = 8.5 \, cm$
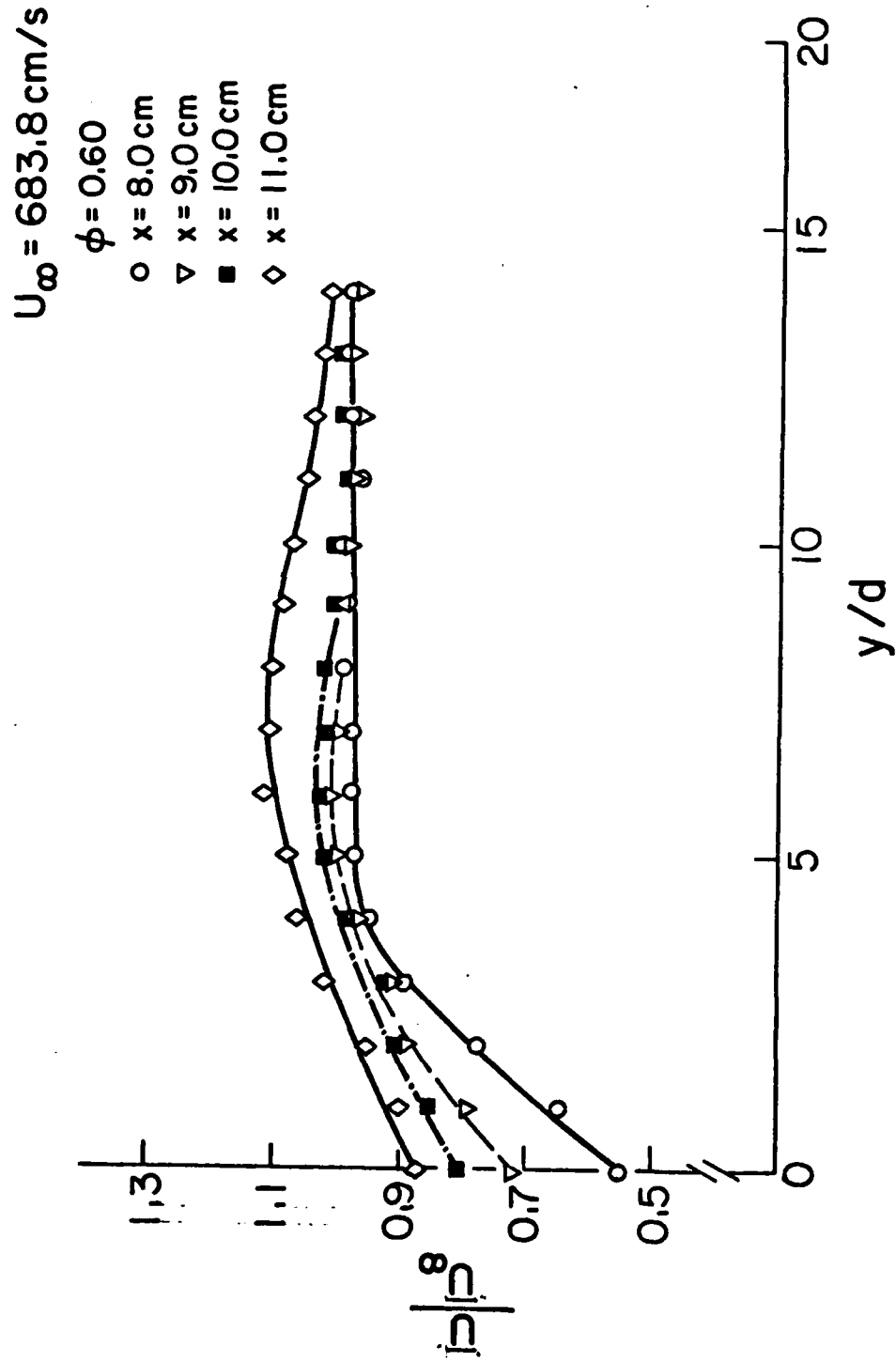
Figure 3.9 MEAN VELOCITY PROFILES THROUGH A FLAME
IN GRID-INDUCED TURBULENCE

XBL 802-367
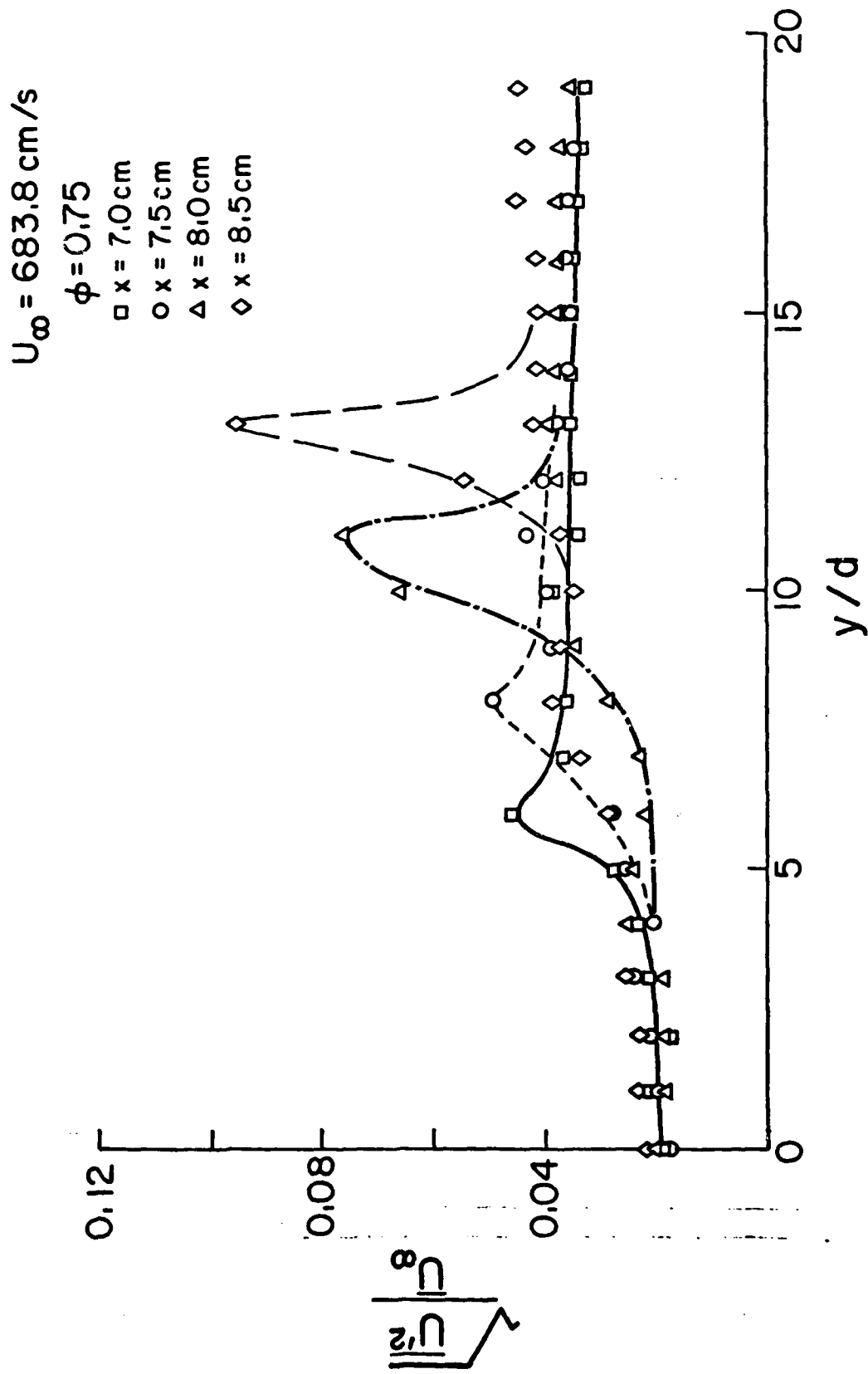
Figure 3.10 TURBULENCE INTENSITY PROFILES THROUGH A
FLAME IN GRID-INDUCED TURBULENCE

XBL 802-370

VELOCITY (CM/S)

U=684 CM/S,PHI=0.75,X=8.5,Y=1.3 CM

640.660.680.700.720.740.760.780.800.820.840.860.880.900.920.

P. D. F.

1.50E-02
1.30E-02
1.10E-02
9.00E-03
7.00E-03
5.00E-03
3.00E-03
1.00E-03
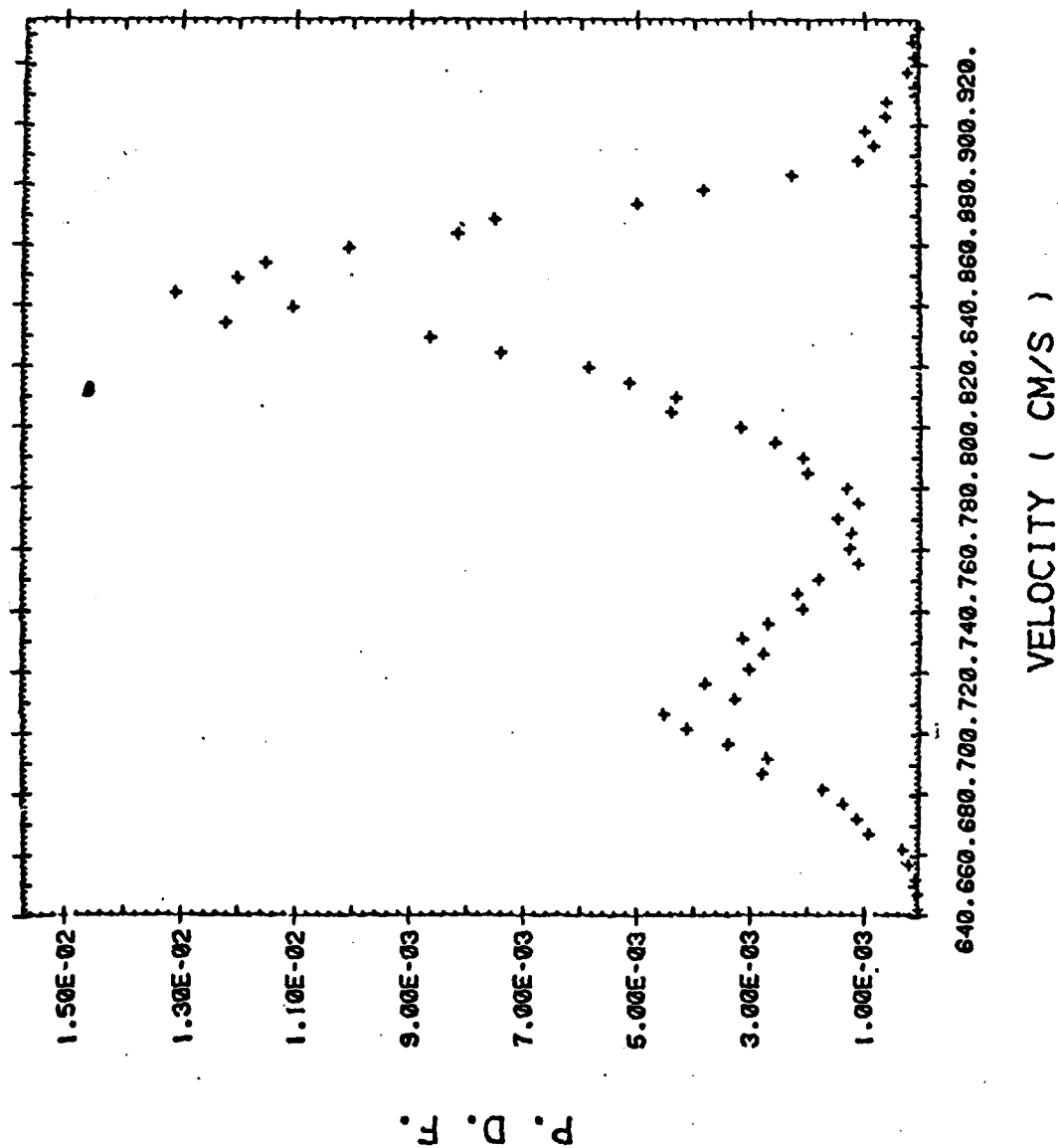
Figure 3.11 PROBABILITY DENSITY FUNCTION OF VELOCITY IN A TURBULENT FLAME FRONT
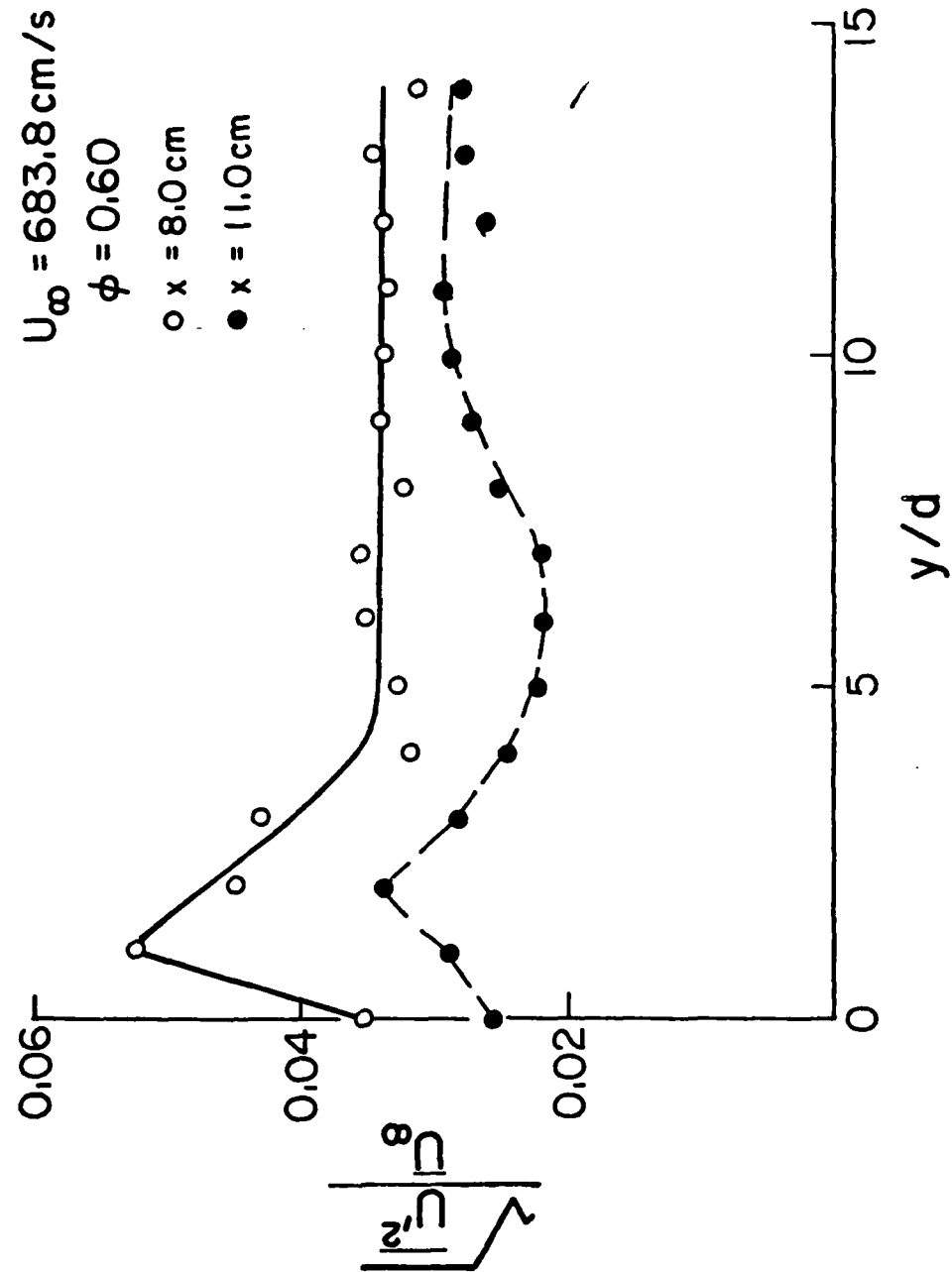
Figure 3.12 TURBULENT VELOCITY INTENSITY
THROUGH A FLAME IN GRID-INDUCED TURBULENCE

XBL 802-372

LOG FREQUENCY
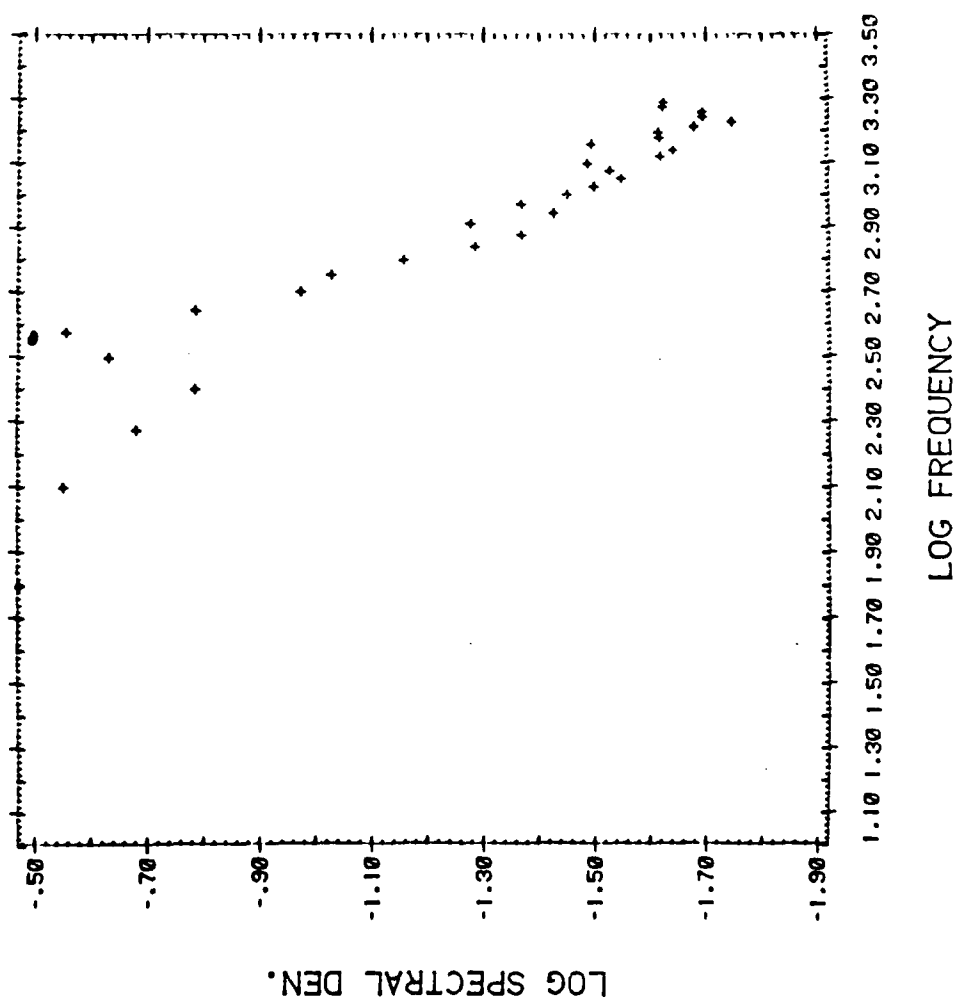
U=684 CM/S,PHI=0.60,X=11.,Y= 5 CM

Figure 3.13 POWER SPECTRUM OF VELOCITY BEHIND A FLAME FRONT

LOG FREQUENCY

U=684 CM/S,PHI=0.75,X=8.5,Y=1.9 CM

Figure 3.15 SPECTRAL DENSITY FUNCTION

TIME DELAY (SEC.)
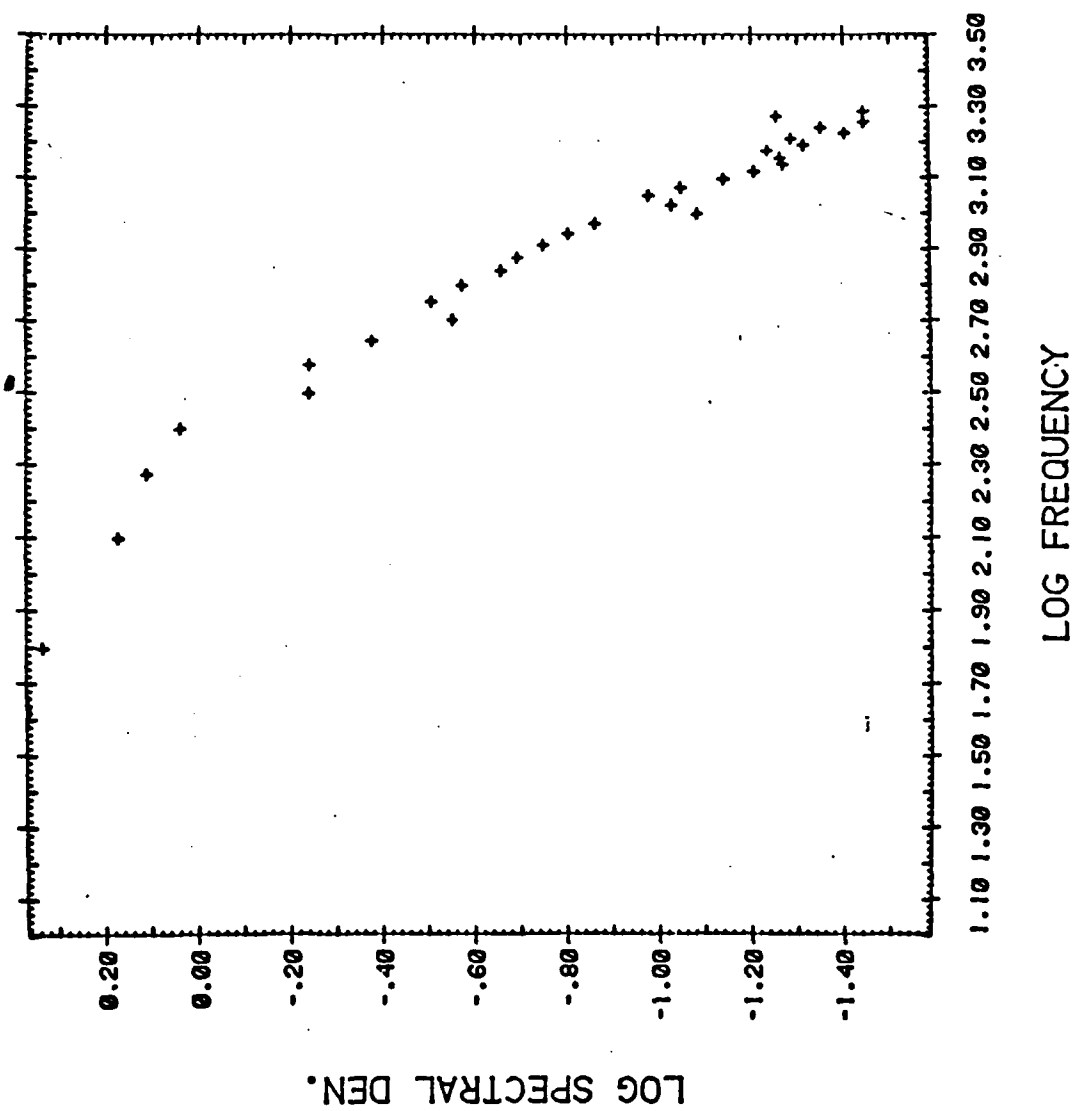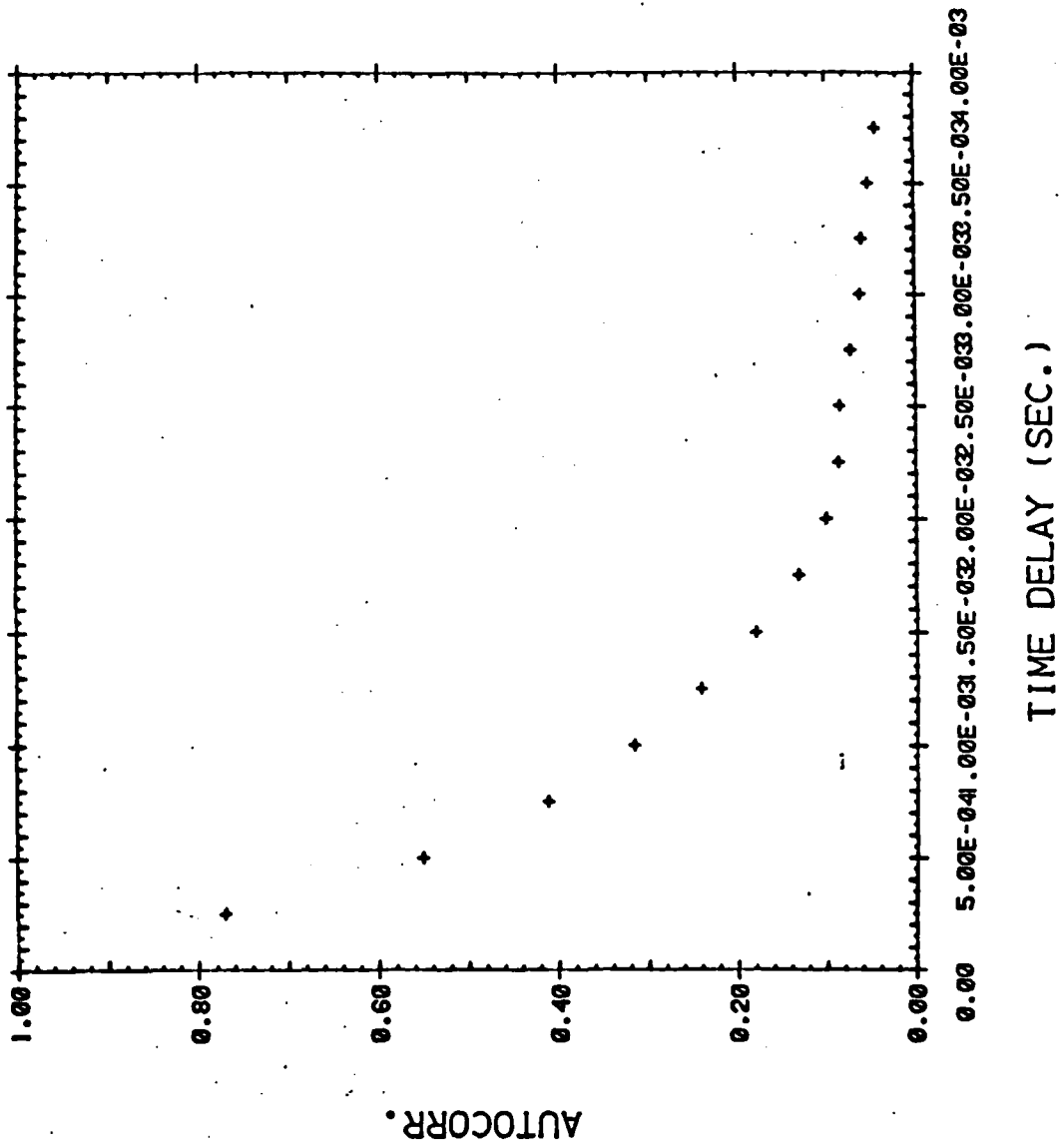
U=684 CM/S,PHI=0.75,X=8.5,Y=1.9 CM

Figure 3.15 AUTOCORRELATION FUNCTION IN GRID-INDUCED TURBULENCE
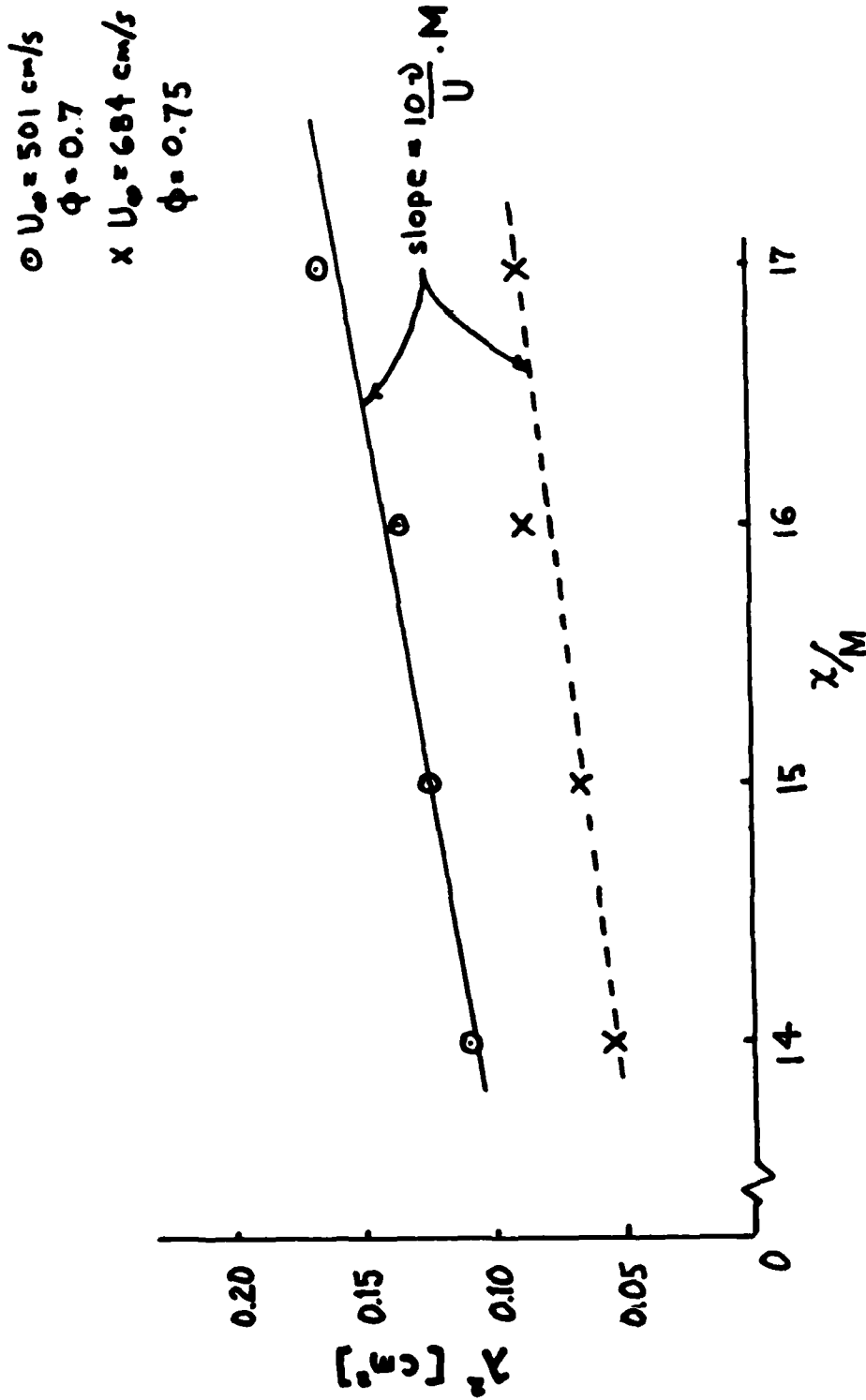
Figure 3.16 EVOLUTION OF THE TAYLOR MICROSCALE, λ, BEHIND A FLAME FRONT PROPAGATING IN GRID-INDUCED TURBULENCE
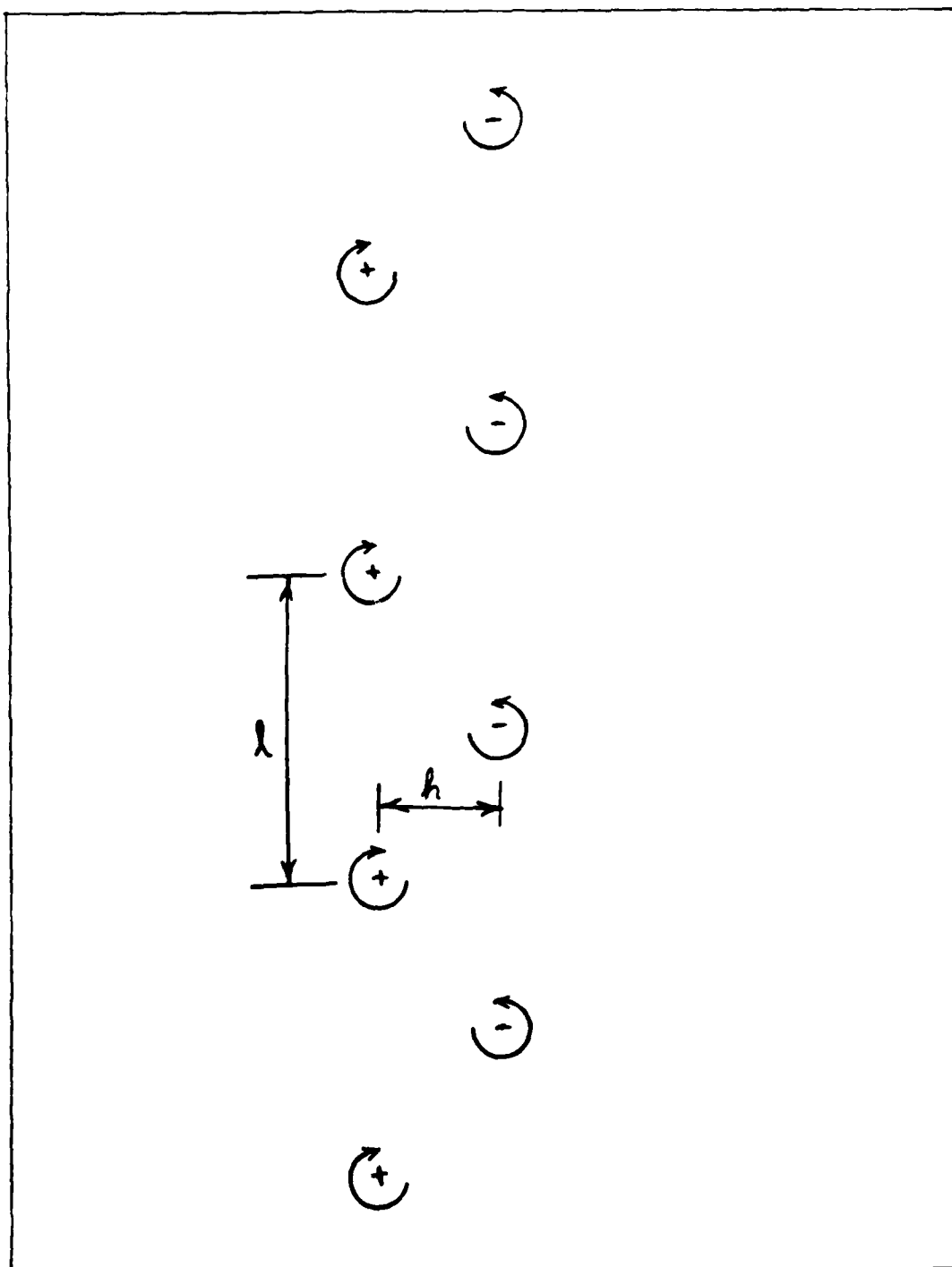
Figure 4.1 - Ideal Kármán vortex street
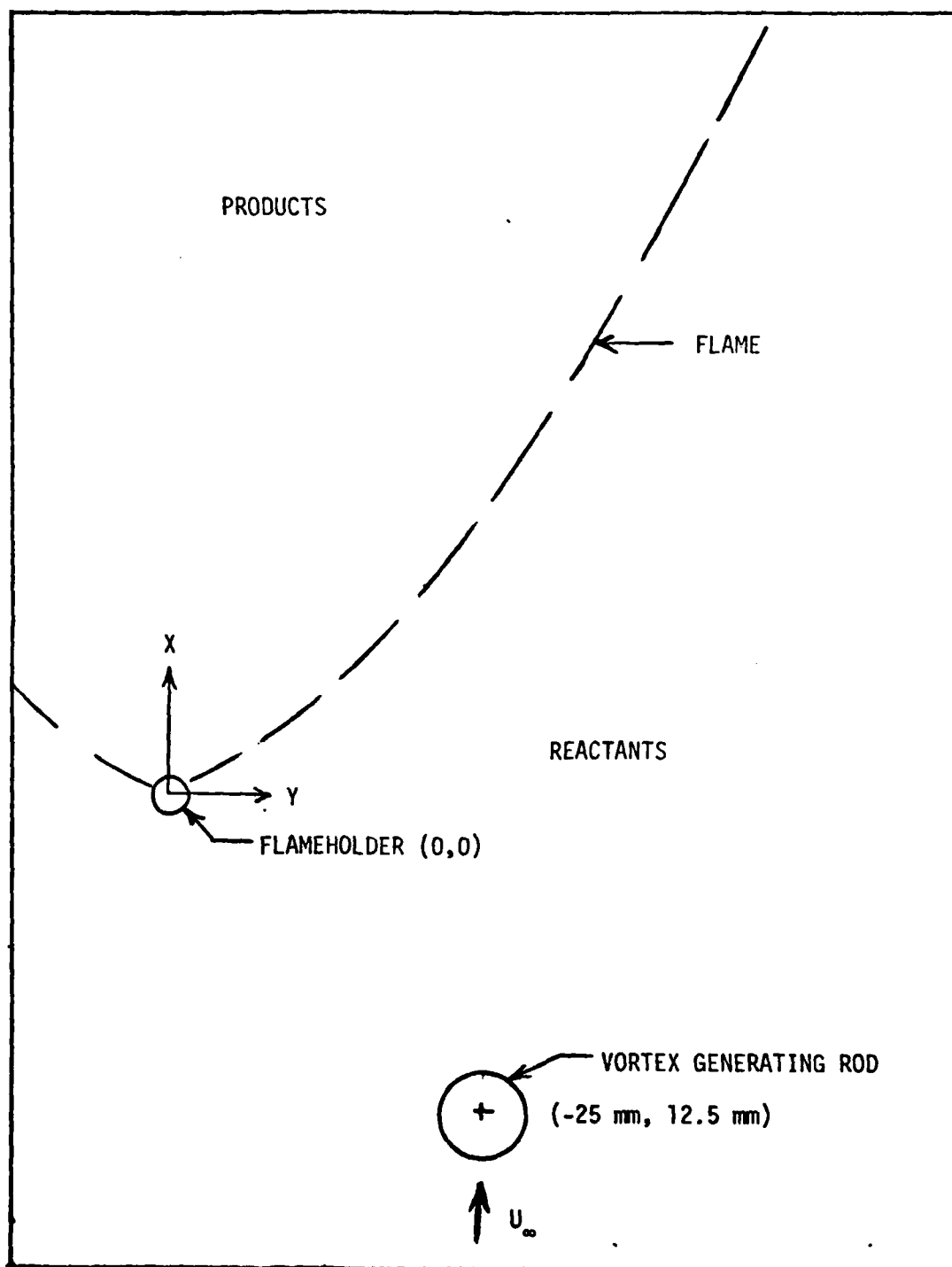
Figure 4.2 - Schematic of flame interaction with a
Kármán vortex street and coordinate system.
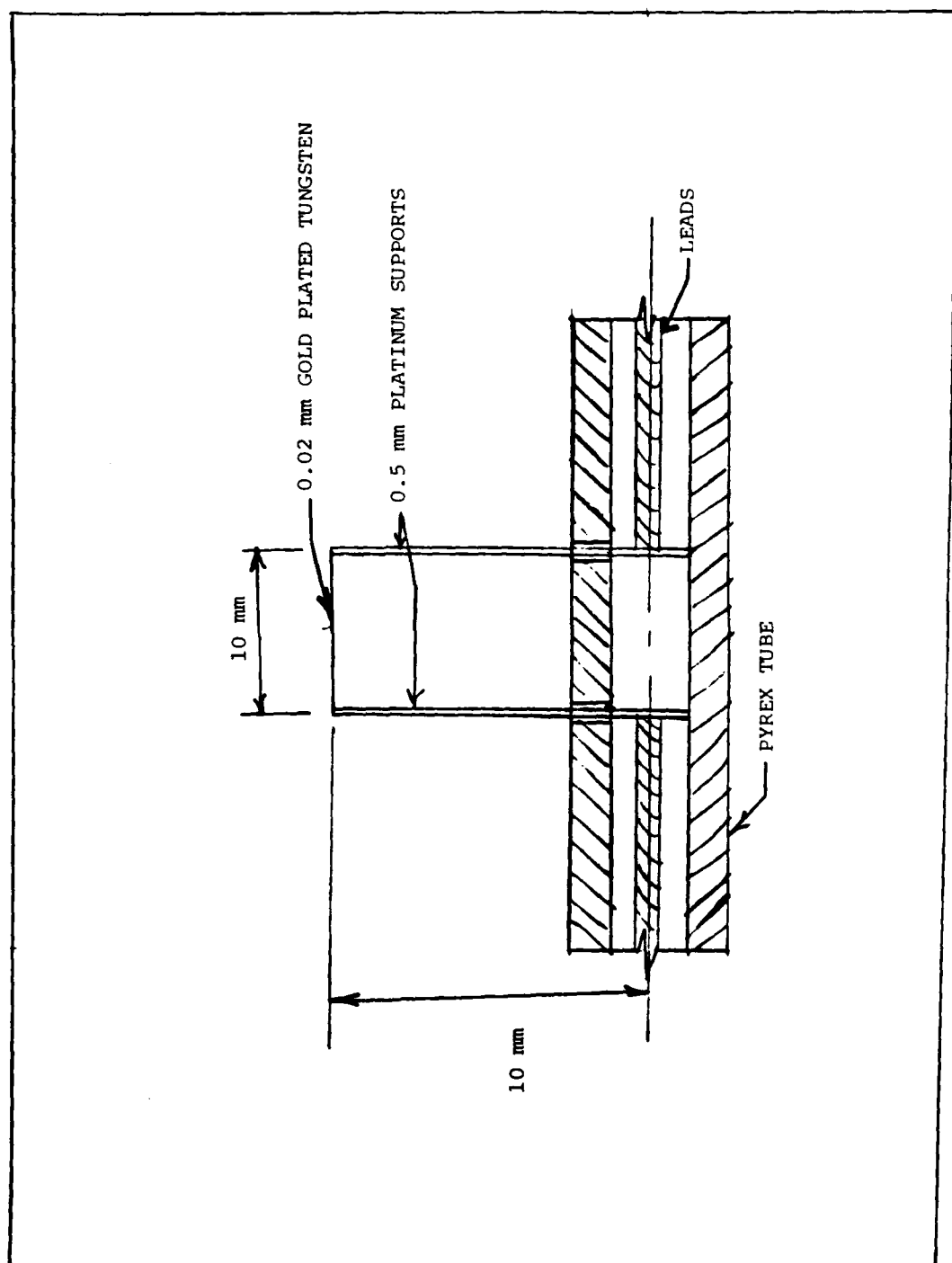
Figure 4.3 – Schematic of vortex generator/reference probe holder.
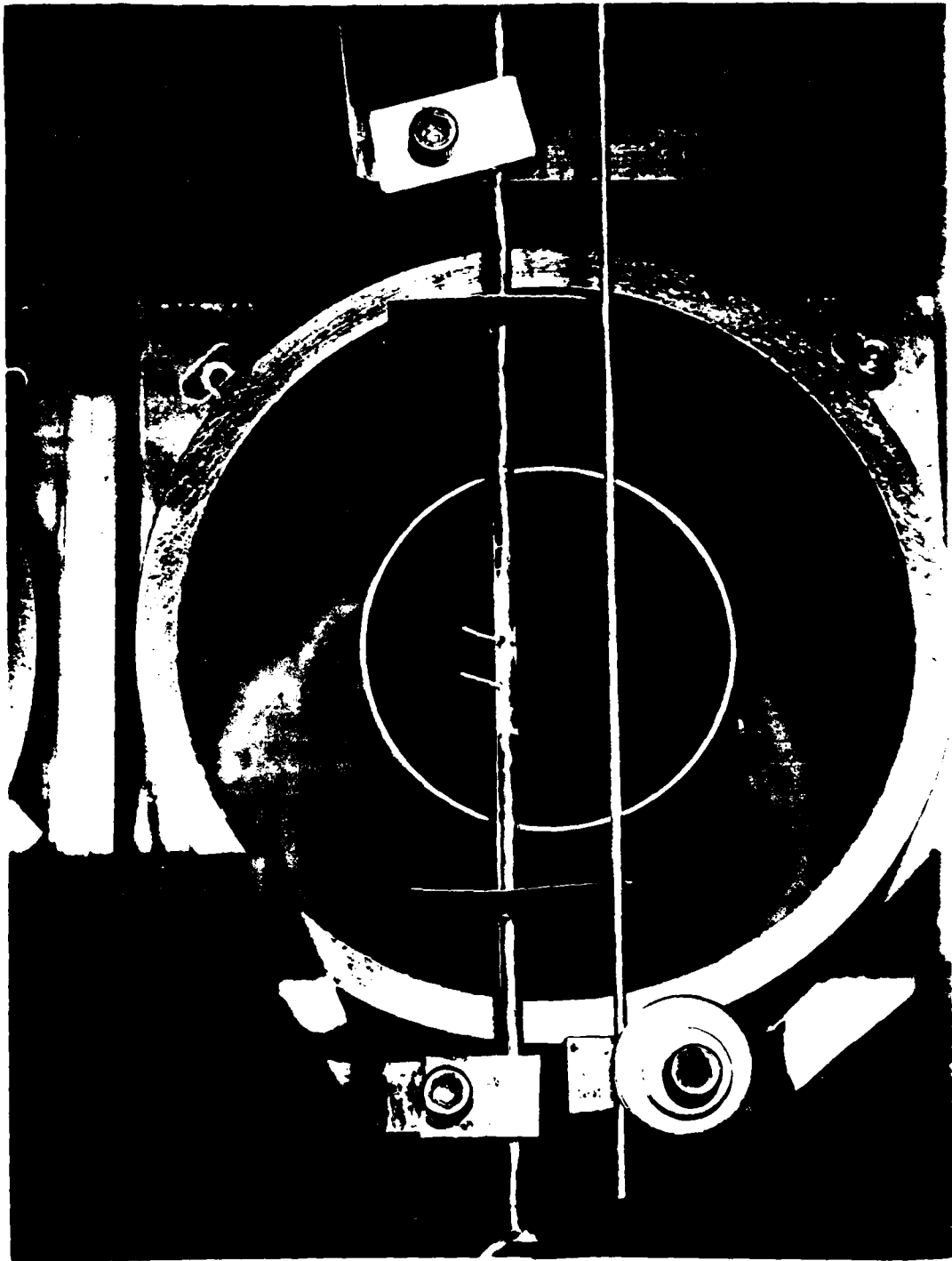
Figure 4.4 - Test section for flame interaction
with a Karman vortex street.

CONSTANT U CONTOURS KARMAN VORTEX STREET

(b)

(a)
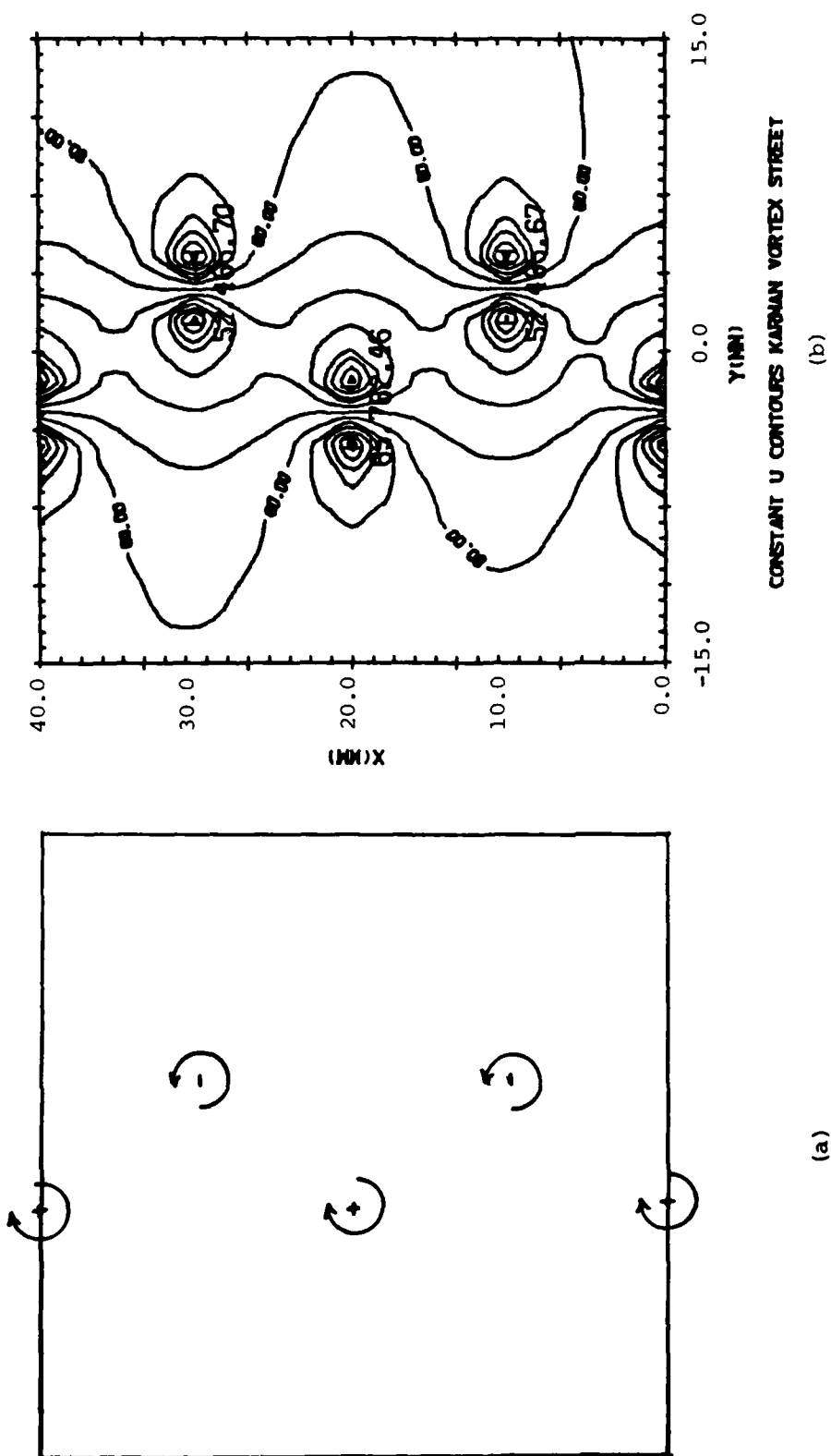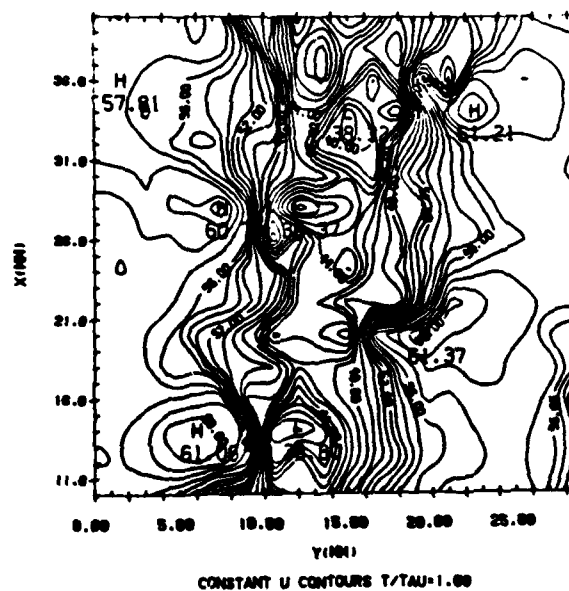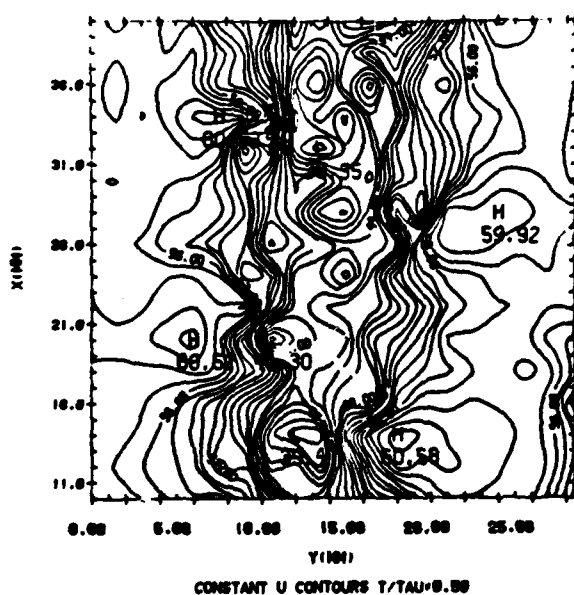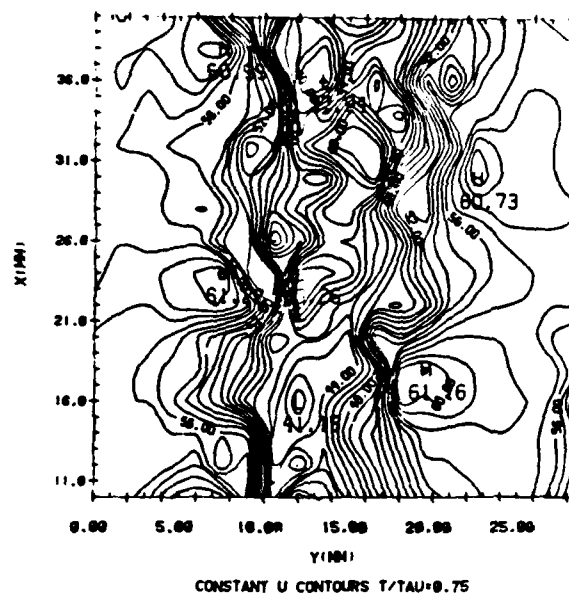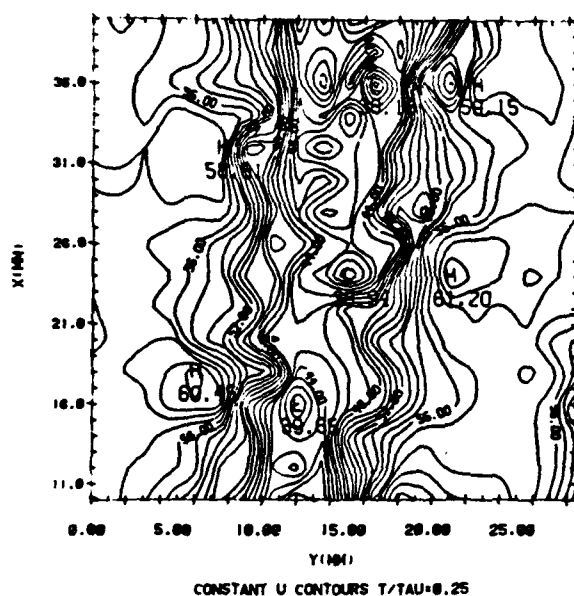
FIGURE 4.5

Figure 4.6 - Streamwise velocity contours
of the wake of 2.0 mm cylinder.
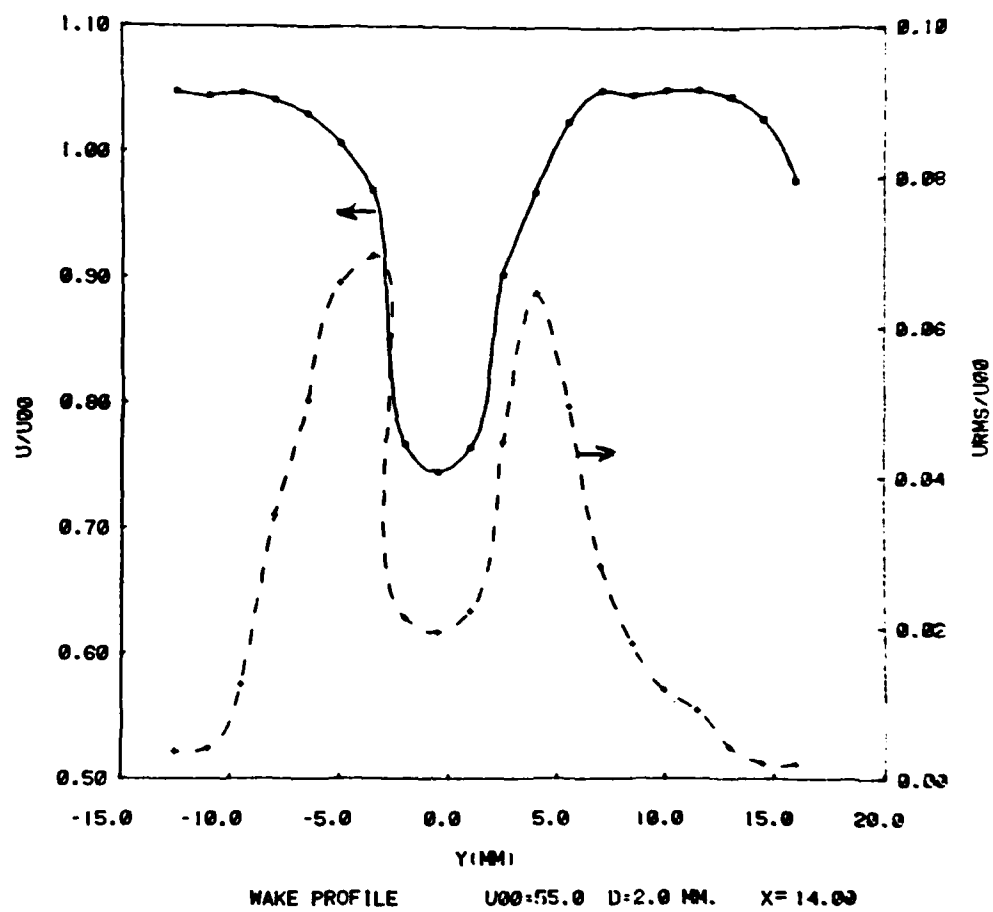
Figure 4.7 - Mean and rms velocity profile in
the wake of 2.0 mm cylinder.
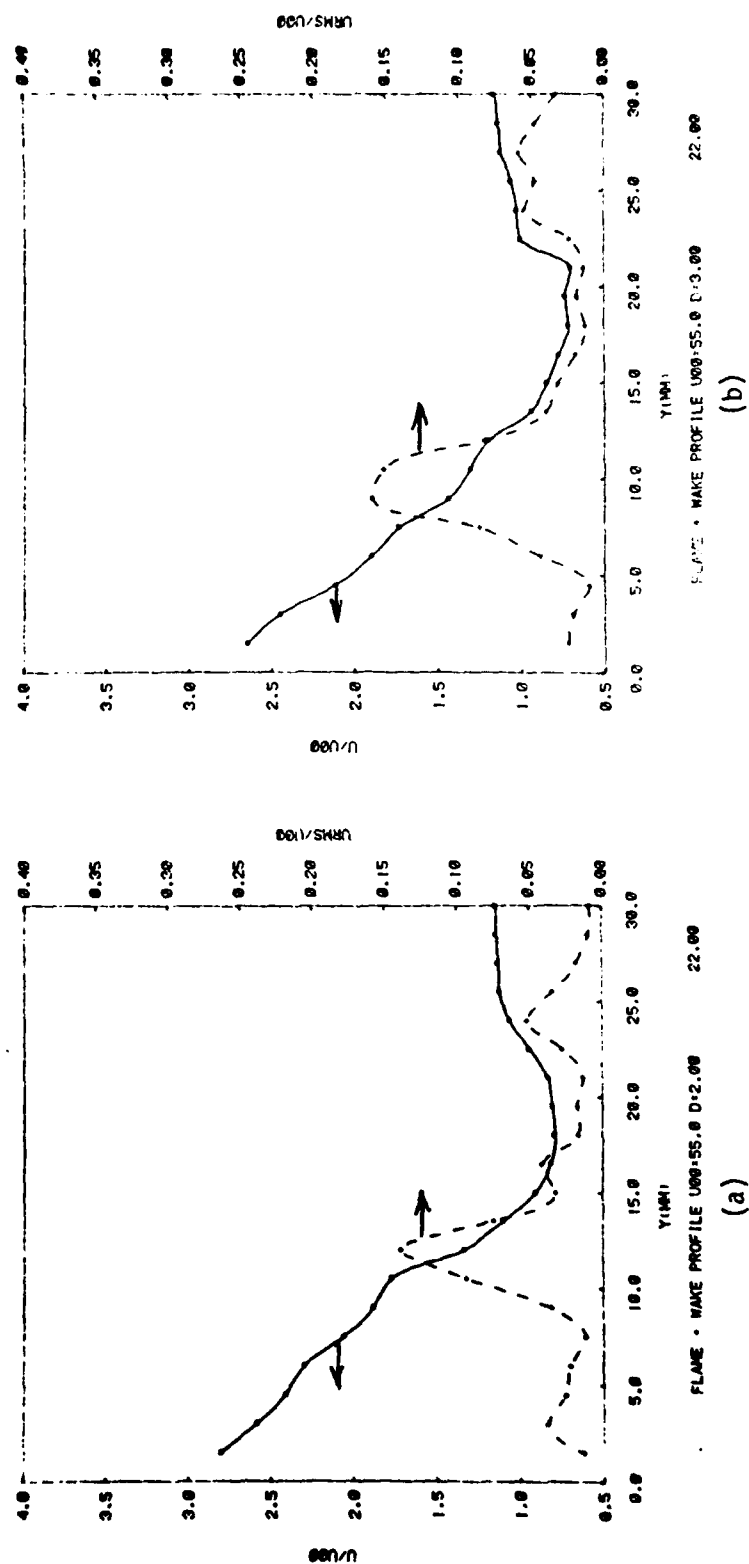
Figure 4.8 - Mean and rms velocity profiles through a
flame in the wake of (a) 2.0 mm cylinder and (b) 3.0 mm cylinder
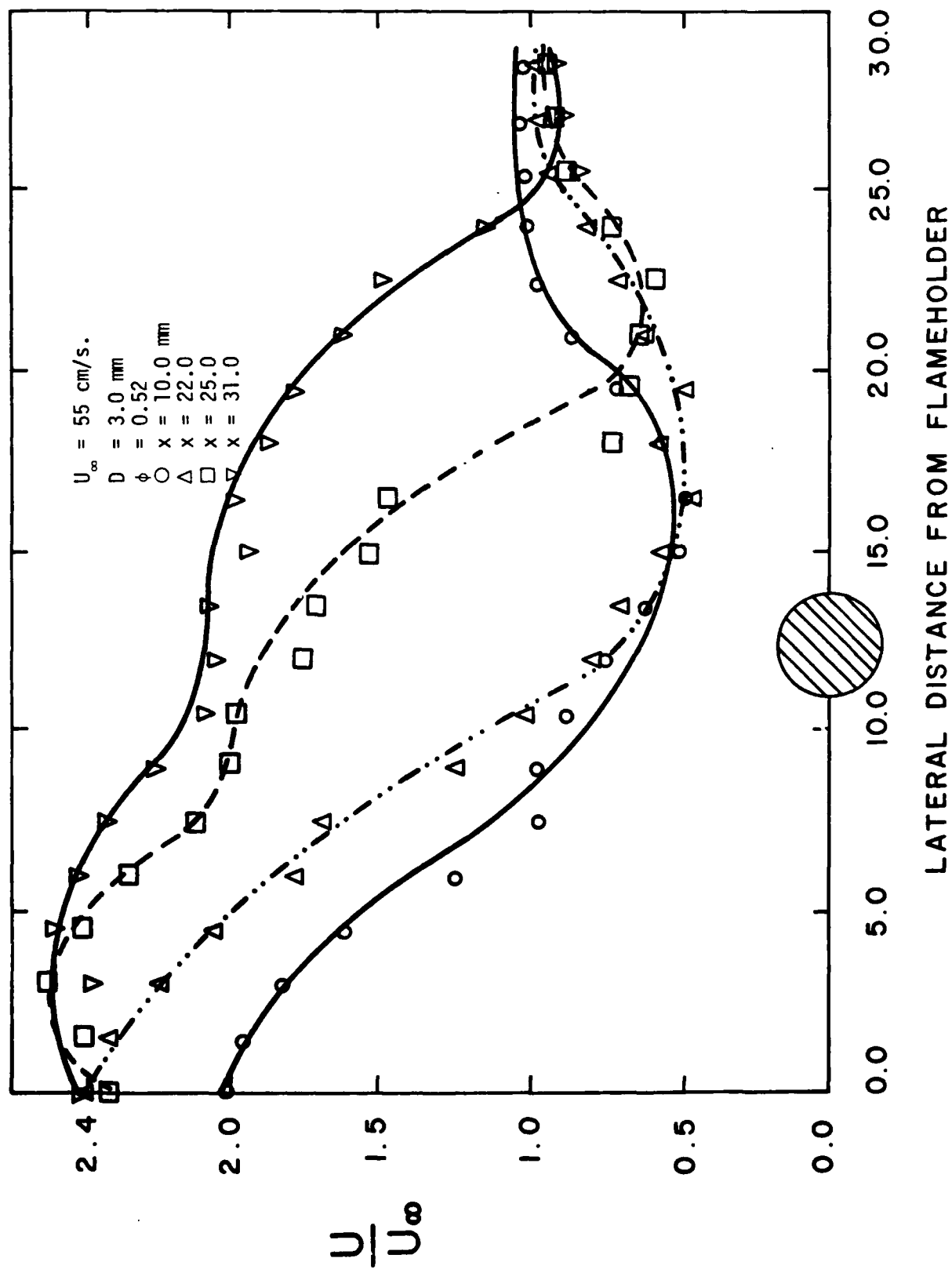
Figure 4.9 - Mean velocity profiles through a flame in the wake.

(a)

(b)
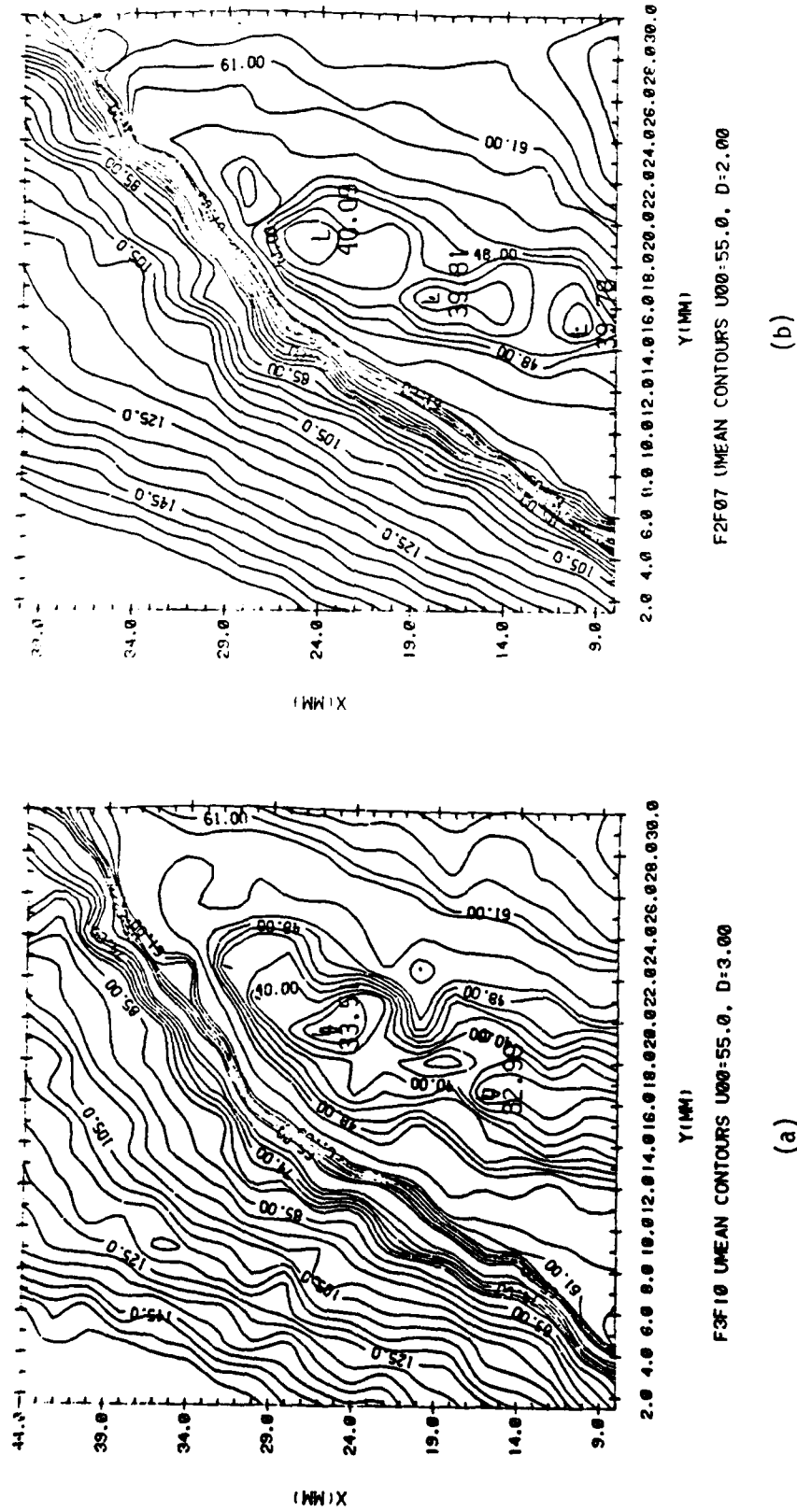
Figure 4.10 - Mean velocity contours for flame in the

wake of (a) 2.0 mm and (b) 3.0 mm cylinder.
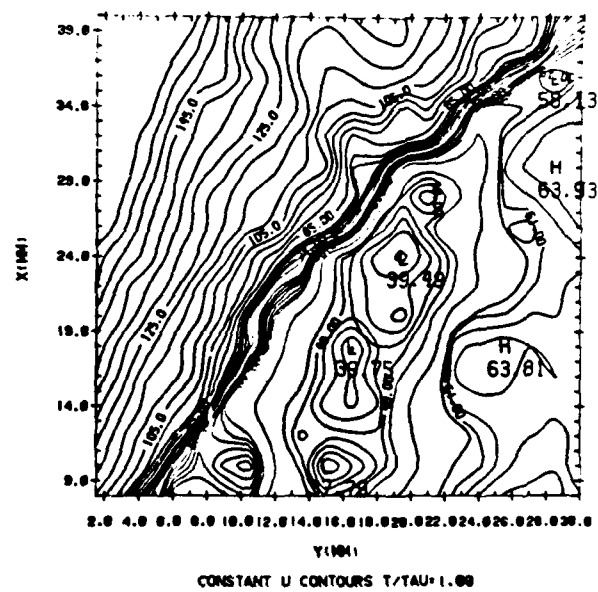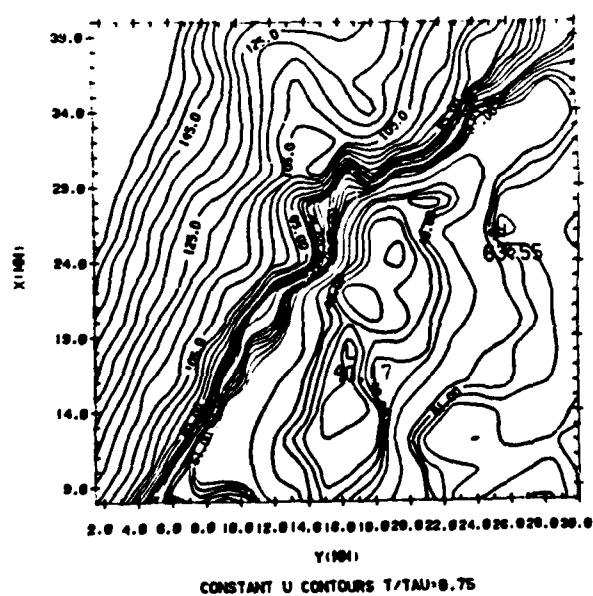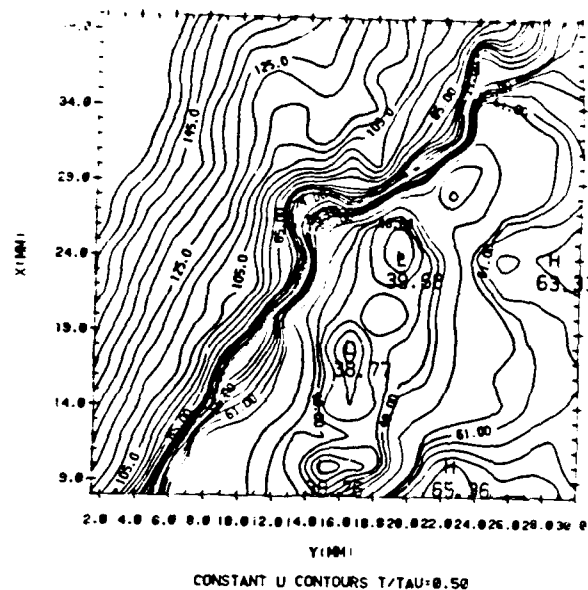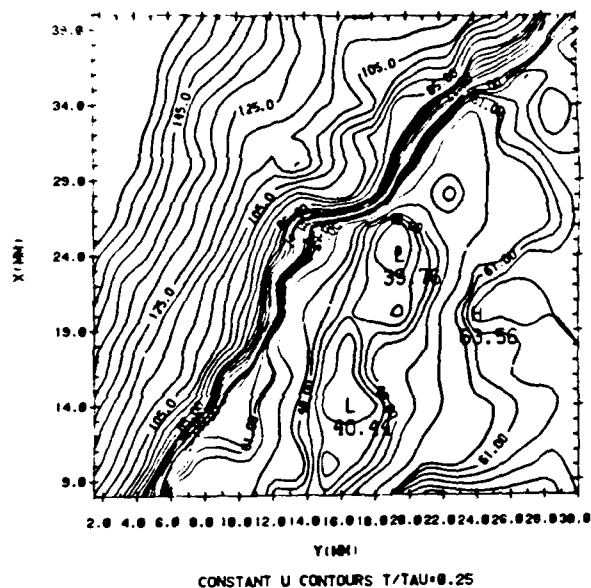
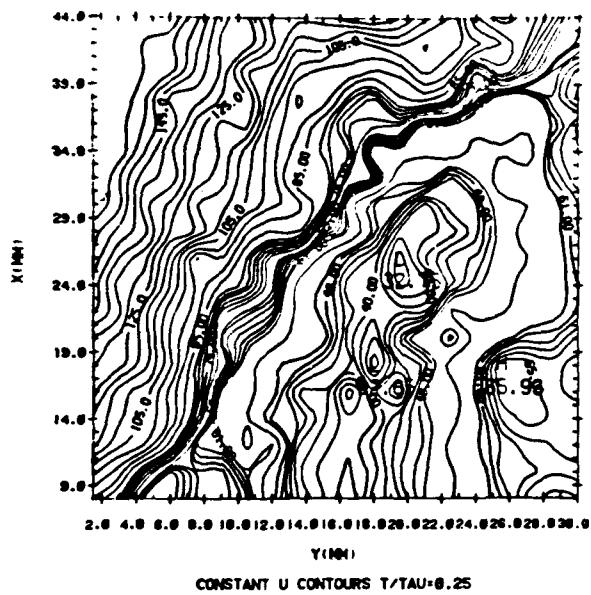Figure 4.11 - Velocity contours through flame

in the wake of 2.0 mm cylinder
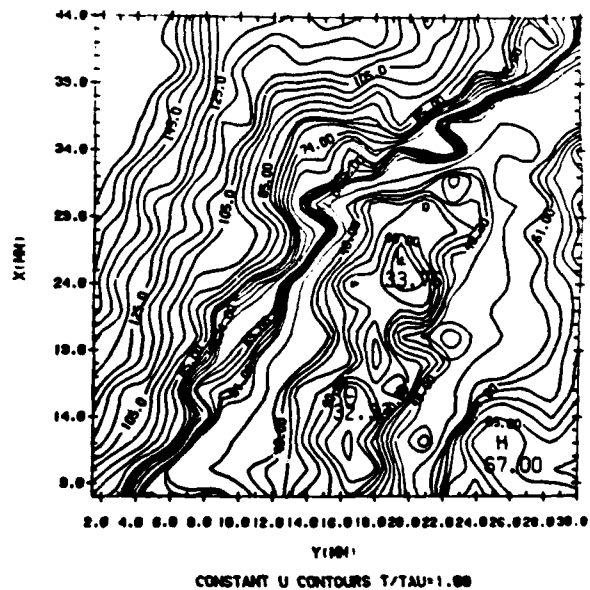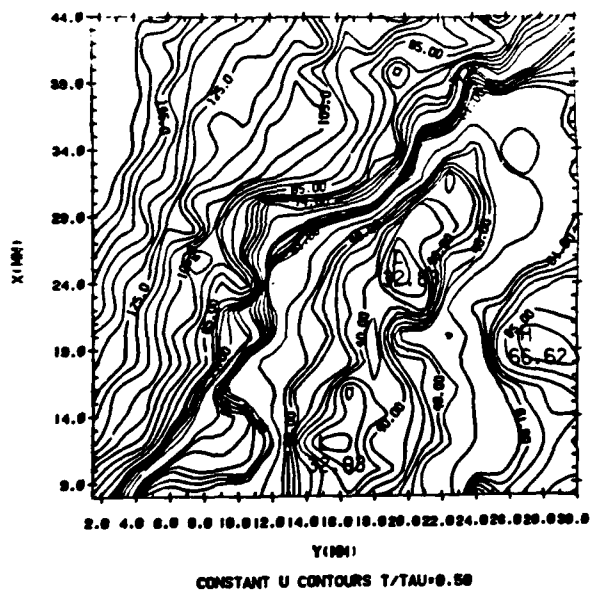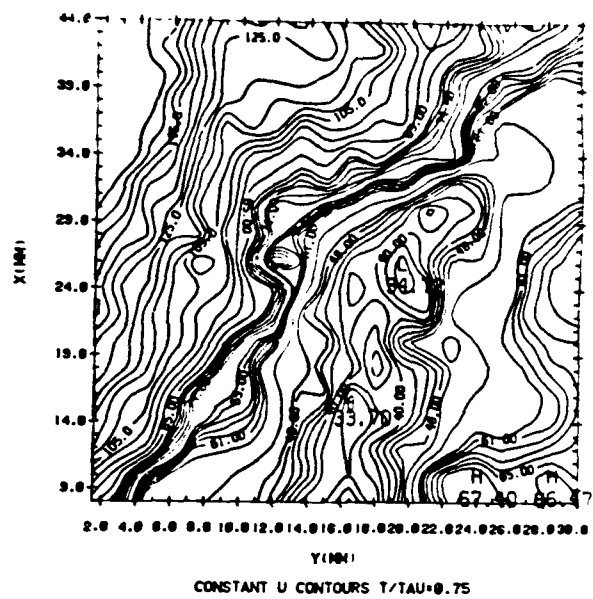
Figure 4.12 - Velocity contours through flame in
the wake of 3.0 mm cylinder

APPENDIX A

NUMERICAL SIMULATION OF THE INTERACTION OF A FLAME WITH A KÁRMÁN VORTEX STREET *

By

I. Karasalo, A. J. Chorin, I. Namer, F. Robben, L. Talbot

University of California, Berkeley and

Lawrence Berkeley Laboratory

Berkeley, CA 94720

APPENDIX B

INTERPRETATION OF RAYLEIGH SCATTERING
IN A FLAME

I. Namer, R. W. Schefer, and M. Chan

University of California, Berkeley
and Lawrence Berkeley Laboratory
Berkeley, California 94720

DATE
ILMED
-8